2013

Legged Self-Manipulation

Aaron Johnson
University of Pennsylvania, aaronjoh@seas.upenn.edu

Daniel E. Koditschek
University of Pennsylvania, kod@seas.upenn.edu

Copyright 2013 IEEE. Reprinted from *Access, IEEE*
Page(s):
310 - 334
ISSN :
2169-3536
INSPEC Accession Number:
13528378
Digital Object Identifier :
10.1109/ACCESS.2013.2263192
Date of Publication :
16 May 2013

Legged Self-Manipulation

Abstract
This paper introduces self-manipulation as a new formal design methodology for legged robots with varying ground interactions...

This work was supported by the ARL/GDRS RCTA project under Cooperative Agreement Number W911NF-10–2–0016.

For further information, visit Kod*lab.

Disciplines
Engineering

Comments
Copyright 2013 IEEE. Reprinted from *Access, IEEE*

Page(s):
310 - 334
ISSN :
2169-3536
INSPEC Accession Number:
13528378
Digital Object Identifier :
10.1109/ACCESS.2013.2263192
Date of Publication :
16 May 2013
Date of Current Version :
30 May 2013
Issue Date :
2013
Sponsored by :
IEEE

Errata Page 310, the citation to prior publication of section IV-A should read [13]. Page 316, Eqn. (17), the subscript on R should read wp. Page 317, Eqn. (29) should be the line just after Eqn. (28). Page 328, Eqn. (68), the length terms in the denominator of the first line should be squared, as in Eqn. (67), and the font for ε in Result C.5 should match this line. Page 330, Appendix D, first column, the sixth line of equations in this section should not include the symbol × (this should be interpreted as the usual matrix multiplication with the previous line). Page 331, Appendix E, first column, the fourth line of equations on this page should not include the symbol × (this should be interpreted as the usual matrix multiplication with the previous line). Page 332, second column, the reference to the mass matrix and Corilis matrix in Fig. 15 should have no equation numbers (81 and 82 are unrelated).

IEEE Access
practical innovations : open solutions

Received April 12, 2013, accepted May 7, 2013, date of publication May 16, 2013, date of current version May 29, 2013.

Digital Object Identifier 10.1109/ACCESS.2013.2263192

Legged Self-Manipulation

AARON M. JOHNSON (Student Member, IEEE), AND DANIEL E. KODITSCHEK (Fellow, IEEE)
Electrical and Systems Engineering Department, University of Pennsylvania, Philadelphia, PA 19104, USA

Corresponding author: A. M. Johnson (aaronjoh@seas.upenn.edu)

This work was supported by ARL/GDRS RCTA Project under Cooperative Agreement W911NF-10-2-0016. Portions of this work, in particular Section IV-A, were previously presented in [1].

ABSTRACT This paper introduces self-manipulation as a new formal design methodology for legged robots with varying ground interactions. The term denotes a set of modeling choices that permit a uniform and body-centric representation of the equations of motion—essentially a guide to the selection and configuration of coordinate frames. We present the hybrid system kinematics, dynamics, and transitions in the form of a consistently structured representation that simplifies and unites the account of these, otherwise bewilderingly diverse differential algebraic equations. Cleaving as closely as possible to the modeling strategies developed within the mature manipulation literature, self-manipulation models can leverage those insights and results where applicable, while clarifying the fundamental differences. Our primary motivation is not to facilitate numerical simulation but rather to promote design insight. We instantiate the abstract formalism for a simplified model of RHex, and illustrate its utility by applying a variety of analytical and computational techniques to derive new results bearing on behaviors, controllers, and platform design. For each example, we present empirical results documenting the specific benefits of the new insight into the robot's transitions from standing to moving in place and to leaping.

INDEX TERMS Legged locomotion, Robot control, Robot kinematics, Manipulator dynamics.

I. INTRODUCTION

Legged robots, such as the notional mechanism in Fig. 1, will necessarily experience a variety of changing contact conditions as they perform ever more complex tasks requiring greater autonomy on novel, and possibly shifting, terrain. As new conditions arise, it is crucial to formally (and therefore automatically) generate and analyze the system dynamics, in a manner requiring as little knowledge as possible about the geometry and mechanics of the substrate. In contrast, multi-fingered object manipulation has been well formalized for many decades [1]–[6], motivating our paper that leverages this established body of work and extends it to legged robots as they manipulate themselves through the world. We exploit these "self-manipulation" modeling choices to generate the diverse constrained quasi-static and Lagrangian dynamics (as well as the hybrid transition conditions that relate them) arising from the exponentially many possible contact conditions. The framework is body centric (does not require full knowledge of the world reference frame), allows for massless limbs (does not require an invertible mass matrix), and permits underactuation (does not require an invertible kinematic Jacobian). More than numerical simulation (e.g. [7]), our goal is the distillation of physically parametrized models into formal design results, utilizing a variety of analytical and numerical methods.

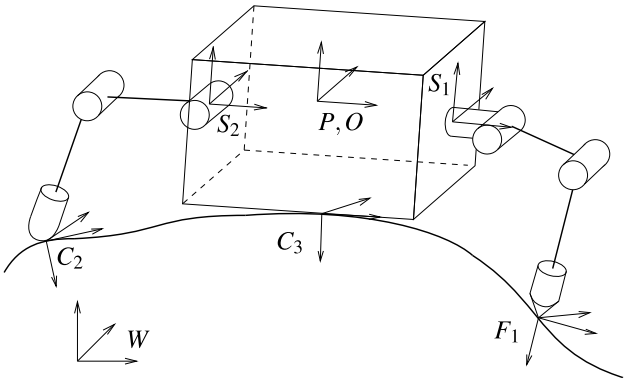

FIGURE 1. Selected coordinate frames for self-manipulation of a legged robot, where the object frame O is connected to the world but co-located with the palm frame P on the robot. Figure adapted from [1, Fig. 5.14].

The central contribution of the paper is summarized in a single "master equation" (33), in addition to the equations and modeling decisions that lead up to it, expressing a rigid

robot's Lagrangian dynamics together with the constraint forces required to sustain them for any combination of legs and other body parts contacting rigid ground. From the perspective of electromechanical platform design, this model elucidates the role of morphology and actuator characteristics in promoting or precluding certain desired motions of the body. From the perspective of behavior design, the model comprises a compact, uniform representation of the hybrid dynamical control system—the family of state spaces, controlled dynamics over them, and guard conditions and reset maps determining their adjacency—that must be exercised to achieve those motions.

The use of this formalism is illustrated with reference to a succession of tasks executed on the RHex robot [8], [9] wherein the interplay of controlled joint torques, leg contact conditions, and body reactions is particularly heightened by that machine's very limited actuation. But the model is applicable to any legged machine, and we are convinced that specific power (W/kg) limitations exhibited by every available actuation scheme [10]–[12] will incur very similar, complex tradeoffs between various limb strategies for imparting work upon the body. We believe that the body-centric self-manipulation framework will reveal deeper, more formal results concerning the adjacency relations between a legged machine's hybrid dynamics cells with strong behavioral implications, but these ideas go beyond the scope of the present paper and are merely hinted at in the conclusion through speculative remarks concerning further work presently in progress.

We intend the paper to be readily accessible to readers acquainted with modern texts on robot manipulation and control [1]–[6]. The modeling principles underlying self-manipulation are quite general, and as such are presented first in tutorial form. We believe their value and coherence is best conveyed in the context of a specific robot presented with a variety of specific tasks, spanning the energetic range from static to quasi-static to dynamic. The RHex robot is required to first stand in place (with the least possible energy on unknown terrain [13]), then manipulate itself in that place (while acting as a "tilt-scanning" sensor platform [14], [15]) and finally leap dynamically from that place (to "prepare" [16] various behaviors such as gap crossing [17] or pronking [18]). The value of this formal method becomes quite apparent when the great multiplicity, diversity and dynamically varying nature of the contact modes is considered across these seemingly disparate tasks. The framework generates automatically the equations of motion for all of them, whose consistent structure differs only in one term (the matrix $\mathbf{A}$ in Eqn. (32)) facilitating not only computational analysis but also formal proofs of the validity or optimality of behavioral choices, controller design, and robot morphology.

This paper is structured as follows: Section I-A compares and contrasts self-manipulation with traditional manipulation and locomotion models. Section I-B then introduces the motivating behaviors which illustrate the benefits of this analysis. Section II formalizes the modeling decisions and then review the quasi-static and dynamic equations of motion. The abstract formalism is instantiated in Section III for RHex, providing a concrete example. This model is put to task in Section IV, where the various behaviors are instantiated and analyzed, with specific new design results called out. Section V concludes the paper with a brief summary and look ahead.

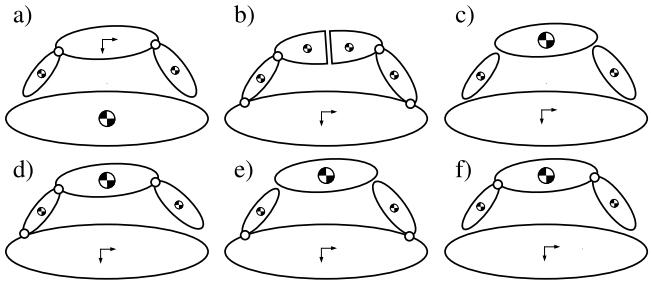

FIGURE 2. Various models for a closed-loop kinematic chain: (a) manipulating the world with your feet, (b) "broken back"—symmetric robots that meet in the middle, (c) free body diagram, (d) "walking model"—single open chain, (e) being manipulated by the world, (f) self-manipulation (used here).

A. BACKGROUND: SELF-MANIPULATION, MANIPULATION, AND LOCOMOTION

Most centrally, the self-manipulation methodology appeals to the key formulation of the manipulation literature, the "grasp map" or "grip transformation", $\mathbf{G}$ [2], which relates wrenches at the contact points to wrenches on the object.[1] Specifically, in Section II-B, we adopt the same modeling choices that lead to this map in the traditional setting. However in self-manipulation, the robot must itself move relative to the inertial world, and we focus attention on the consequences of this departure from the manipulation framework.

Of course such modeling decisions are not required to arrive at accurate kinematics or dynamics. Consider the robot in Fig. 2, a single kinematic chain similar to a 4 bar mechanism. The robot could be "cut" in many ways, in order to determine the identical e-DOF (degrees of freedom, here $e = 1$) from various q-dimensional open-loop dynamics and c constraint forces. For example, one might make: one cut, at a toe ($q = 3, c = 2$, Fig. 2(d), common in walking analysis [19], [6, Ch. 16]) or at the robot center ($q = 4, c = 3$, Fig. 2(b), producing strong symmetries); two cuts at the hips ($q = 5, c = 4$, Fig. 2(e), akin to parts feeding [20]) or at the toes ($q = 5, c = 4$, Fig. 2(a), direct instantiation of manipulation [21], [22], as well as Fig. 2(f), sometimes called a "floating-base" [23]); four cuts, at the joints ($q = 9, c = 8$, Fig. 2(c), a free body diagram). Each variation of this example results the same one-DOF mechanics model, however cutting at the toes (Fig. 2(f)) admits simple expressions for friction at each toe (as opposed to at the hip or body, Fig. 2(b), (e)),

[1] We adopt the specific notation introduced in [1], though these ideas coincide with the formulation in [2]–[6]—and, indeed, most works on the subject make similar modeling decisions.

generalizes across all contact conditions (as opposed to the walking model which must be separately instantiated in each mode, Fig. 2(d)), and with far fewer states and constraints than the more general problem (Fig. 2(c)).

Contrary to the oft encountered adage, locomotion is not the *same* as manipulation. To any reasonable level of precision, a legged robot is not moving the world with its feet (i.e. the ''object'' is Earth,[2] Fig. 2(a), [21], [22]), nor is the world moving the robot (i.e. grounded legs reaching up and manipulating the robot Fig. 2(e), [20]). In particular there are three main differences between the usual manipulation formulation and the self-manipulation setting: the robot is the object (and so the ''Palm'' and ''Object'' frames are coincident, as in Fig. 1); we are concerned with motion of the robot and not what the robot is touching (and so the grasp map must be composed with an appropriate reflection, as appears in (15)); and the dynamics of the legs and body are not decoupled (so in particular the mass matrix is no longer block diagonal, as apparent in (25), complicating the dynamics). Why bother following a manipulation formulation if the problems are actually different? While not every result carries over exactly, the problems are similar enough that matching as closely as possible the modeling decisions that have emerged from this very successful and mature body of work facilitates the reuse, or slightly modified extension, of several valuable ideas and results (e.g. rolling contact [24]–[28], Section II-F).

Finally, it is worth a brief pause to consider the relationship between self-manipulation and locomotion, though they are often considered equivalent [29]. Typically, the locomotion problem domain focuses on the mobility of the body in machines or animals [30], and, most commonly, with respect to a greatly reduced or ''template'' [31] projection (although certainly not always, e.g. [19]). In contrast, the self-manipulation problem is to determine the simplest ''anchor'' [31] that fully expresses the actuators' abilities perform to work upon that body, typically via ground reaction forces directed through the limbs (16), but, not unimportantly, often through momentum transfer in flight (67). Our ''master equation'' (33) formulates the self-manipulation problem under conditions of great enough generality to provide a complete anchoring model for virtually any locomotion problem where the substrate mechanics is well characterized by traditional lumped models (e.g. excluding flowing media [32]).

B. RESULTS: CONTROLLERS, BEHAVIORS, DESIGNS

We illustrate the utility of the self-manipulation formalism through a succession of increasingly energetic tasks implemented on the decade-old hexapod, RHex [8], [9]. The selected behaviors hopefully strike the reader as a plausible and coherent short ''episode'' of a kind likely to arise within an autonomous missions: the robot comes to a halt at some location of interest; once there, it actively engages its sensory payload; this new information provokes the sudden determination to leap up and escape that location. Notwithstanding the intuitively straightforward, even mundane nature of this simple vignette, in the absence of a systematic formalism along the lines this paper develops, such a succession of tasks would present the behavior designer with a diverse (and combinatorially numerous) array of seemingly unrelated mechatronic and sensorimotor control problems whose common implementation offers no unifying insight into what properties of the platform might help or hinder the mission. In contrast, we point out how this general methodology informs and simplifies the analysis of each of these constituent tasks regarded separately, and affords a unifying framework for analyzing the performance as a function of platform design parameters (here focused on leg shape [33], [34], but the formalism makes explicit the role of the various other morphological parameters (e.g., Table 2) in the behavioral consequences).

1) REACTIVE STANDING

The first behavioral example (Section IV-A) seeks to find a reduction in the power needed for stand-in-place tasks on unmodeled rough terrain [13]. The controller developed is quite simple and implements the intuitive notion that all actuators must resist external load while relaxing any relative imbalances between their individual efforts. However it is not immediately apparent under what circumstances this scheme is correct, nor even that it converges in all application situations. The analytical expression for internal and external torques facilitates the identification of the appropriate operating conditions and a proof of convergence assuming they prevail. As this proof covers both round and stick legs, the design choice makes no real difference for this behavior. The controller provides up to a 90% reduction in power use compared to an open-loop stand.

Why worry about the power used when the robot is idle? In one urban search and rescue study researchers discovered that for 49% of the robot's deployment it remained stationary, as the operators needed that time to gain situational awareness [35]. This is corroborated by RHex tests in the Mojave desert, where in at least one specific instance during a trial in March of 2010, the operator paused the robot in a standing posture while deciding how to proceed, causing a motor to burn out after less than a minute. Robots operating on challenging terrain, especially in the heat of a desert, need a low-energy standing posture for health and mission runtime.

2) PITCHING SENSOR SWEEP

For almost any exteroceptive task, perceptual capability can be increased by extending a sensor's field of view by moving it. Rather than (or in addition to) adding dedicated ''neck'' actuators, Section IV-B documents how RHex's legs can be used to provide a change in pitch, increasing the vertical field of view of any payload. Here the formal setup of the constraints in different contact modes determines analytically both the pitching range as well as the pitching velocity in any mode. Furthermore the dynamical liftoff conditions provide a

[2] ''The planet Earth's radius and mass are R_0 and M_0,'' [22].

speed bound for safe execution.

Our empirical example of this general idea features a horizontal (Dorsal) planar laser scanner, a sensor that has no vertical extent and so the only way to build a two dimensional depth map is to move it out of the plane. Prior work on this behavior used an ad-hoc geometric model of the half circle legs to numerically compute an operable scanning range of about 10° [14]. Without an analytical form, the geometry would have to be re-generated in each contact state. It turns out that this behavior benefits from a different contact mode (with the body sliding on the ground). Furthermore while both round and stick legs can reach this same peak pitch, the rounded legs require less torque to do so. Since the kinematics and dynamics are analytically derived with this formalism across all contact states, the pitching velocity can be controlled, and the maximal velocity the behavior can execute without breaking ground contact is found to be higher in the sliding contact mode. The final behavior has a range of $\pm 17°$ that can be used for example to more easily detect stairwells and cliffs [15].

3) PITCH CONTROL IN LEAPING

Recent work has raised the question of how best to use a leap to "prepare" [16] a subsequent behavior by reaching some goal state, whether that goal is across a gap, onto an obstacle, or continuing into another leap [17]. In this prior work, individual actuators were assigned a trivial control policy (maximal torque), and the varied sequences of contact modes achievable through their relative timing dictated the resulting state. Here we consider a finer use of the actuators over the course of a prescribed route through the contact modes (notionally motivated by gap crossing or pronking [18], [36]) wherein the robot must at some point engage all its legs on the ground and reach an aerial state with large forward but low pitching kinetic energy.

We analyze three aspects of pitch control for such leaps in Section IV-C—the behavior design (focusing on the splay or the asymmetry in leg angle), the controller design (focusing on stubbing the toes and using the legs as tails), and the robot design (focusing on the shape and the mass of the legs). The underlying dynamics of a splayed posture is beneficial in several ways. While pushing with both legs equally maintains a level pitch at first, the front leg provably break its ground contact first, and so the robot pitches upwards. A splayed leap (as used before and adjusted via hand tuning [18], touchdown plane control [36], or exhaustive search [17]) minimizes this liftoff imbalance. Furthermore a splayed pronk has the added benefit of a higher possible velocity.

The best results for pronking on RHex have all resorted to decelerating or stubbing the rear legs near the end of stance [36], [37]. We show analytically that this negative work does cut down the pitch of the robot, though at the same time bleeding off some of the forward kinetic energy, as demonstrated experimentally in an extreme case.

Next, to illustrate the role of leg design in leaping, the dynamics are combined with the takeoff conditions in single support to derive a bound on maximum forward velocity. This bound suggests that the rounded leg design of RHex enables a higher maximum speed than an equivalent stick leg. Furthermore we consider the inertial effects of the nearly massless legs [38], which in the air act as "tails," [39], [40], that are able to generate a non-trivial body rotation.

II. SELF-MANIPULATION

A. NOTATION

Table 1 summarizes the notation in this section, chosen where possible to match [1]. Denote a rigid frame B, expressed in the coordinates of rigid frame A (or, equivalently, a rigid transformation that takes frame A into frame B) $\mathbf{g}_{ab} \in \mathcal{G}_a := SE(\mathrm{d})$, where $d = 2$ for a planar model and $d = 3$ for a spatial model. In local coordinates a rigid transformation will be written as a vector, for example $\mathbf{x} = [x, y, z, \phi_y, \phi_p, \phi_r]^T$, where the Euler angles may be chosen as convenient but here will be ZYX—Yaw, Pitch, Roll. The group product will be denoted as $\mathbf{g}_{ab} \cdot \mathbf{g}_{bc}$. The velocity of frame B relative to frame A as seen by A is $\mathbf{V}^s_{ab} = \dot{\mathbf{g}}_{ab} \cdot \mathbf{g}^{-1}_{ab}$, or in twist coordinates $\left[\begin{smallmatrix} v^s_{ab} \\ \omega^s_{ab} \end{smallmatrix}\right]$ (the "spatial" velocity), while the same velocity written in the coordinates of frame B is $\mathbf{V}^b_{ab} = \mathbf{g}^{-1}_{ab} \cdot \dot{\mathbf{g}}_{ab}$ (the "body" velocity) [1, Section 2.4.2]. A body wrench (generalized force), $\mathbf{F}_b := \left[\begin{smallmatrix} f \\ \tau \end{smallmatrix}\right]$, is defined such that work is $\mathbf{V}^b_{a,b} \cdot \mathbf{F}_b$. An adjoint transformation matrix, $\mathbf{Ad}_{g_{ab}} : T\mathcal{G}_a \to T\mathcal{G}_b$, relates the two expressions of velocity, $\mathbf{V}^s_{ab} = \mathbf{Ad}_{g_{ab}} \mathbf{V}^b_{ab}$ [1, Chapter 2].

Denoting by π_x a projection down to the x component, π_{c_k} a projection to some collection of components to be defined by the friction conditions as specified below, and the non-subscripted π the projection from an element of $SE(\mathrm{d})$ (position and orientation) to $\mathbb{R}^{\mathrm{d}}$ (position only), we express the origin of a frame, $\mathbf{g}$, as (e.g. when $d = 2$) $(x, z) = \pi(\mathbf{g}) \in \pi(\mathcal{G}) \approx \mathbb{R}^2$. Similarly let $\mathrm{R}_{ab} = \pi_R \mathbf{g}_{ab}$ be the rotational component of the rigid transformation, in matrix form. To convert between local coordinates and twist coordinates, define (e.g. when $d = 2$), $\mathbf{R} := \left[\begin{smallmatrix} \mathrm{R} & 0 \\ 0 & 1 \end{smallmatrix}\right]$, so that $\mathbf{V}^b_{ab} = \mathbf{R}^T_{ab} \dot{\mathbf{x}}$.

B. MODELING DECISIONS

This self-manipulation model follows the usual conventions from manipulation [1]–[6]: the hand and object are separated at the fingertips; the wrench bases at the fingers (i.e. the motions that the contact resists) are considered in unison; and (through the separated velocity constraints of the grasp map and hand Jacobian) dictate the forces and torques on the object and robot. However since the robot is the object, we set the "Object" frame, O, to be coincident with the robot's "Palm" frame, P.

Define the following coordinate frames, as shown in Fig. 1 (and corresponding to [1, Fig. 5.14]). Let P be attached to the COM of the robot body segment, and the object frame, O be co-located at P, but attached to the world. The usual manipulation problem takes the palm frame as fixed, and so from the robot's perspective it appears that the gravitational force is applied to the movable Earth (the object), and not the

TABLE 1. Key symbols used throughout this paper, with section or equation of introduction noted.

$\mathrm{a} := \lvert \mathrm{n} - \mathrm{e} \rvert \in \mathbb{Z}^+$	Internal or uncontrolled DOF (II-H)
$\mathbf{a} : \mathcal{Q} \to \mathcal{C}$	Base Constraint Function (9)
$\mathbf{A} : T\mathcal{Q} \to T\mathcal{C}$	Velocity Constraint Function (11)
$\mathbf{Ad}_{g_{ab}} : T\mathcal{G}_a \to T\mathcal{G}_b$	Adjoint transformation from a to b (II-A)
$\mathbf{B}_{c,k} : T^*\mathcal{C}_k \to T^*\mathcal{G}_{c_k}$	Wrench basis at contact (3)
$\mathrm{c} = \dim(\mathcal{C}) \in \mathbb{Z}^+$	Number of active contact wrenches (II-C)
$\mathbf{C} : T\mathcal{Q}^2 \to T^2\mathcal{Q}$	Coriolis matrix (30)
$C_k \in \mathcal{G}_c$	Contact frames (ground aligned) (II-C)
$\mathcal{C}_k \subset \mathcal{G}_{c_k}, \mathcal{C} = \Pi_k \mathcal{C}_k$	Space of contact positions (II-C)
$\mathrm{d} \in \{2, 3\}$	Dimension of model (planar or spatial) (II-A)
$\mathbf{D} : T\mathcal{Q} \to T^2\mathcal{Q}$	Coriolis & internal dynamics (33)
$\mathbf{E} : T^*\mathcal{Q} \to T^2\mathcal{Q}$	Applied & external dynamics (33)
$\mathrm{e} = \mathrm{q} - \mathrm{c} \in \mathbb{Z}^+$	Unconstrained DOF (II-G)
$\mathbf{f} \in T^*\mathcal{C}$	Contact wrench magnitudes (6)
$\mathbf{F}_a \in T^*\mathcal{G}_a$	Generalized force (wrench) (II-A)
$F_k \in \mathcal{G}_f$	Finger frames (leg aligned) (II-C)
$\mathbf{g}_{ab} \in \mathcal{G}_a := SE(\mathrm{d})$	Rigid transformation from A to B (II-A)
$\mathbf{G}_s : T^*\mathcal{C} \to T^*\mathcal{G}_p$	Self-manipulation grasp map (15)
$\mathbf{h} : \mathcal{Y} \to \mathcal{Q}, \mathbf{H} := D\mathbf{h}$	Implicit kinematic mobility function (18), (19)
$\mathbf{J}_h : T\Theta \to T\mathcal{C}$	Hand Jacobian (16)
$\mathbf{J}^s_{sf} : T\Theta \to T\mathcal{G}_c$	Finger Jacobians (II-E)
$\mathcal{K} \subseteq \mathbb{Z}^+, \mathrm{k} = \lvert \mathcal{K} \rvert$	Set of active contact points (1)
$L : T\mathcal{Q} \to \mathbb{R}$	Lagrangian (28)
$L_k \in \mathcal{G}_l$	Leg segment frame (leg aligned) (II-C)
$\mathbf{M}_a : T^2\mathcal{G}_a \to T^*\mathcal{G}_a$	Mass matrix (25)–(26)
$M_k \in \mathcal{G}_m$	Motor frames (leg aligned) (II-B)
$\mathrm{n} = \dim(\Theta) \in \mathbb{Z}^+$	Number of joints (II-B)
$\mathbf{N} : \mathcal{Q} \to T^*\mathcal{Q}$	Nonlinear forces (gravity) (31)
$O \in \mathcal{G}_o$,	Object frame (coincident with P) (II-B)
$P \in \mathcal{G}_p$	Palm frame (body aligned) (II-B)
$\mathrm{q} = \mathrm{n} + \mathrm{d}(\mathrm{d}+1)/2 \in \mathbb{Z}^+$	Dimension of the combined state (II-B)
$\mathbf{q} \in \mathcal{Q} := \Theta \times \mathcal{G}_o$	Combined system state (II-B)
$\mathrm{R} \in SO(\mathrm{d})$	Rotation Matrix (II-A)
$S_k \in \mathcal{G}_s$	Leg attachment frames (body aligned) (II-B)
$T : T\mathcal{Q} \to \mathbb{R}^+$	Kinetic Energy (24)
$\mathbf{U} : T^*\mathcal{C} \to \mathbb{R}^{\mathrm{k}}$	Friction cone (4)
$\mathcal{U} \subseteq \mathbb{S}^1$	Range of angles considered (II-B)
$v \in T\pi\mathcal{G}$	Linear velocity (II-A)
$V : \mathcal{Q} \to \mathbb{R}^+$	Potential energy (27)
$\mathbf{V}^s_{ab} \in T\mathcal{G}_a, \mathbf{V}^b_{ab} \in T\mathcal{G}_b$	Generalized velocity (twist) (II-A)
$W \in \mathcal{G}_w$	World inertial frame (II-B)
$\mathbf{x} \in \mathcal{G}$	Body position and orientation (II-B)
$\mathbf{x}_c \in \mathcal{C}$	Contact location in the contact basis (5)
$\mathbf{y} := \psi(\mathbf{q}) \in \mathcal{Y}$	Lagrangian free variables (II-G)
$\alpha \in \mathbb{R}^{\mathrm{a}}$	Internal force magnitude (22)
$\zeta \in \mathbb{R}$	Height function (II-I)
$\theta \in \Theta := \mathcal{U}^{\mathrm{n}}$	Joint angle vector (II-B)
$\lambda \in T^*\mathcal{C}$	Lagrange multipliers (constraint forces) (29)
$\pi : SE(\mathrm{d}) \to \mathbb{R}^{\mathrm{d}}$	Projection down to linear components (II-A)
$\tau \in T^*\Theta$	Torque (II-A)
$\Upsilon \in T^*\mathcal{Q}$	External forces (including torques) (31)
$\phi \in SO(\mathrm{d})$	Body Orientation (II-B)
$\psi : \mathcal{Q} \to \mathcal{Y}, \mathbf{Y} := D\psi$	Lagrangian free variable map (II-G)
$\omega \in TSO(\mathrm{d})$	Angular velocity (II-A)

other way around. Co-locating the object and palm coordinate frames allows for wrenches and twists that are referenced to that point in the world, and the robot's actual motion is simply be the opposite sign (from a ground based observation), as explored below. The true world inertial frame, W, is at some unknown but fixed location relative to the ground, and aligned with gravity. The position of the robot, $\mathbf{g}_{wp} \in SE(\mathrm{d})$, or $\mathbf{x}$ when written in local coordinates, is part of our state but we strive to not necessarily need to know anything other than the robot orientation relative to gravity, $\phi \in SO(\mathrm{d})$.

Each leg attaches at a frame fixed on the robot body, S_i for leg i, and for each joint of that leg j a rotating frame that moves with the motor, $M_{i,j}$, at the center of the joint but rotated by $\theta_{i,j} \in \mathbb{S}^1$ about some joint axis (although it may be convenient to restrict the available angles to $\theta_{i,j} \in \mathcal{U}$, for example $\mathcal{U} := [-30°, 30°]$). Denote by $\mathbf{g}_{s_i m_{i,j}}(\theta_{i,1}, \ldots, \theta_{i,j})$ this open-chain kinematic mapping from $\mathbb{T}^j$ into the appropriate rigid group. Define a "leg" frame, $L_{i,j}$, at the center of mass of link and a "finger" frame, F_i, at the toe and fixed relative to the final leg segment. The collection of n total joint angles, $\theta \in \Theta$, combined with the COM position define our overall state, $\mathbf{q} = [\theta \quad \mathbf{x}] \in \mathcal{Q} := \Theta \times \mathcal{G}_o \equiv \mathbb{T}^{\mathrm{n}} \times SE(\mathrm{d})$, having dimension $\mathrm{q} := \mathrm{n} + \mathrm{d}(\mathrm{d}+1)/2$.

C. CONTACT CONDITIONS

In order to determine which parts of the robot are in contact with the ground we first define a contact frame, C_i, at each potential contact point (toe or other body part, and located at F_i in the case of a toe). The contact frame is typically oriented with the $\mathbf{z}$ axis pointing into the object, however here the object being manipulated is the robot. We choose to keep the definition consistent with respect to the legs, and so the $\mathbf{z}$ axis points into the ground (which on flat terrain aligns C_i with W). Note that body contact under this system simply involves a zero jointed "leg" with an appropriate contact frame. Section II-F extends these ideas to rolling contact.

Which contact points are active can be determined by checking the distance to the surface of the local world, with contact of some sort occurring when that distance is zero [6, Section 27.2] (the type of contact is specified below). This condition can be reduced to checking the contact point height, $\zeta_{c_i}(\mathbf{q}) := \pi_z(\mathbf{g}_{c_i w}) - \hat{\zeta}_{c_i}$, for some local terrain height $\hat{\zeta}_{c_i}$ (where $\hat{\zeta}_{c_i} := 0$ for flat level ground). Call the set of k active contact point indices $\mathcal{K}$, such that,

$$\mathcal{K} := \{k | \zeta_{c_k}(\mathbf{q}) \equiv 0\}. \tag{1}$$

The set can be updated inductively if the current contact conditions are known by checking the friction conditions (defined below) on all active contact points and the touchdown conditions on all non-active contact points. The set of contact conditions for a quasi-static RHex is needed in the analysis of Section IV-B (see Fig. 4—and these boundary conditions are used throughout) however it is important to note that none of the control—algorithms we develop in this paper require that

the robot actually know anything about their location.

There are a number of different types of contact possible once a contact point is known, for example RHex has both sliding and non-sliding point contacts (see [2, Table 2–3], [1, Table 5.2] for a full list of examples). In each contact frame define a subspace consisting of only the degrees of freedom that friction keeps fixed, $\mathcal{C}_k \subseteq \mathcal{G}_{c_k}, k \in \mathcal{K}$, with a projection (whose expression in coordinates is a sub-block of the identity matrix), $\mathbf{x}_{c_k} := \pi_{c_k}(\mathbf{g}_{c_k w})$. However the standard grasping analysis instead focuses on the wrenches that the contact can resist (as is required for the non-holonomic constraints of rolling contact), and so in that spirit define the *wrench basis* as the image of the pullback of π_{c_k} from the allowable contact wrenches to all possible contact wrenches at a contact point point [1, Section 5.2.1], $\mathbf{B}_{c_k} : T^*\mathcal{C}_k \to T^*\mathcal{G}_{c_k}$, (written in coordinates, $\mathbf{B}_{c_k}^T := D\pi_{c_k}$). The contact conditions enforce zero motion in these directions as well—giving rise to the familiar dual pairing,

$$\dot{\mathbf{x}}_{c_k} = \mathbf{B}_{c_k}^T \mathbf{V}_{w,c_k}^b, \qquad \dot{\mathbf{x}}_{c_k} \in T\mathcal{C}_k \tag{2}$$

$$\mathbf{F}_{c_k} = \mathbf{B}_{c_k} \mathbf{f}_{c_k}, \qquad \mathbf{f}_{c_k} \in T^*\mathcal{C}_k. \tag{3}$$

This contact constraint holds only when the contact forces are in some Coulomb friction cone relating the normal and tangential forces,[3]

$$\mathbf{U}_k(\mathbf{f}_{c_k}) \geq \mathbf{0}, \quad \mathbf{U}_k : T^*\mathcal{C}_k \to \mathbb{R}^{\mathrm{c_k}} \tag{4}$$

[1, Section 5.2.1], [6, Section 27.3], satisfying,

$$\mathbf{U}_k(\mathbf{f}_a) \geq 0, \quad \mathbf{U}_k(\mathbf{f}_b) \geq 0$$
$$\Rightarrow \ \mathbf{U}_k(\alpha \mathbf{f}_a + \beta \mathbf{f}_b) \geq 0 \quad \forall \alpha, \beta \in \mathbb{R}^+$$

which in the planar case ($d = 2$) is simply a matrix multiplication, $\mathbf{U}_k \mathbf{f}_{c_k} \geq 0$.

For multi-finger robots, and now multi-legged robots, it is often convenient to deal with the collection of contact positions (and similarly for twists and wrenches) among all contact points,

$$\mathbf{x}_c := (\mathbf{x}_{c_1}, \ldots, \mathbf{x}_{c_n}) \in \mathcal{C} := \Pi_{k \in \mathcal{K}} \mathcal{C}_k \tag{5}$$

$$\mathbf{f}_c := (\mathbf{f}_{c_1}, \ldots, \mathbf{f}_{c_n}) \in T^*\mathcal{C} \tag{6}$$

$$\mathbf{U}(\mathbf{f}_c) := (\mathbf{U}_1(\mathbf{f}_{c_1}), \ldots, \mathbf{U}_n(\mathbf{f}_{c_n})) \geq \mathbf{0} \tag{7}$$

where $\mathrm{c} := \dim(\mathcal{C}) = \sum_{k \in \mathcal{K}} \dim(\mathcal{C}_k)$ is the total number of constraints on the system.

D. KINEMATIC LOOP CLOSURES

The friction holding the contact points in place along some dimensions sets up the following constraint functions, expressing the k^{th} contact condition by the equality,

$$\mathbf{x}_{c_k} = \pi_{c_k}(\mathbf{g}_{c_k w}(\mathbf{q})) = \pi_{c_k}\left(\mathbf{g}_{c_k s_k}(\mathbf{q}) \cdot \mathbf{g}_{s_k w}(\mathbf{x})\right) \tag{8}$$

(see further discussion in the Appendix Section A), motivating the definition of the constraint function

$$\mathbf{a}_k(\mathbf{q}) := \pi_{c_k}\left(\mathbf{g}_{c_k w}(\mathbf{q})\right) - \hat{\mathbf{x}}_{c_k} \tag{9}$$

[3]The given frame convention for the $\mathbf{z}$ axis of C_k means that the normal forces are negative in general, see Appendix (76), (78).

whose zeros, $\mathbf{a}_k^{-1}[0]$, comprise the constraint set for some initial contact position $\hat{\mathbf{x}}_{c_k}$. Collectively, the c kinematic constraints are,

$$0 \equiv \mathbf{a}(\mathbf{q}). \tag{10}$$

This constraint sets up the initial pitching sensor behavior presented in Section IV-B.1, though this is quickly extended to include rolling contact as described in Section II-F.

E. INFINITESIMAL KINEMATICS: THE GRASP MAP AND HAND JACOBIAN

The infinitesimal kinematics over the base constraint (10), relates wrenches and twists between the body and joints and contacts, through induced tangent constraints. Given a constrained motion, $\mathbf{q}_a(t) : \mathbb{R} \to \mathcal{Q}$, satisfying (10), $\mathbf{a} \circ \mathbf{q}_a \equiv 0$, these induced constraints can be given coordinate expression by differentiating the constraint equation, however by using the fact that the constraint equation must be true no matter where the world frame is, some of the interdependence is removed. Therefore we claim that,

$$\frac{d}{dt}\mathbf{a}_k \circ \mathbf{q}_a \equiv 0$$
$$\Rightarrow \mathbf{A}_k(\mathbf{q})\dot{\mathbf{q}} := [-\mathbf{B}_{c_k}^T \mathbf{Ad}_{g_{c_k f_k}} \mathbf{J}_{s_k f_k}^b \quad -\mathbf{B}_{c_k}^T \mathbf{Ad}_{g_{c_k p}} \mathbf{R}_{wp}^T]\dot{\mathbf{q}} \equiv 0 \tag{11}$$

where the leg Jacobian $\mathbf{J}_{s_k f_k}^b$ is defined such that, $\mathbf{V}_{s_k f_k}^b = \mathbf{J}_{s_k f_k}^b(\theta)\dot{\theta}$. The proof of this claim may be written out using either a homogeneous representation or a twist representation, as shown in the Appendix Section A. Here instead we show that this equality (11) is equivalent to the standard manipulation constraint,

$$\mathbf{J}_h \dot{\theta} = \mathbf{G}^T \mathbf{V}_{po}^b \tag{12}$$

[1, Eqn. 5.15], typically derived directly in terms of twists by defining the grasp map and hand Jacobian, and not by differentiating a base constraint (10).

In manipulation literature, the *grasp map*, $\mathbf{G} : T^*\mathcal{C} \to T^*\mathcal{G}_o$, takes wrenches at the contact points (i.e., forces at the contact points), $\mathbf{f}_c \in T^*\mathcal{C}$ to wrenches on the object, $\mathbf{F}_o \in T^*\mathcal{G}_o$, and its dual, $\mathbf{G}^T$, acts covariantly, taking body twists of the object, $\mathbf{V}_o \in T\mathcal{G}_o$, to twists at the contact point, $\dot{\mathbf{x}}_c \in T\mathcal{C}$, all expressed in coordinates as,

$$\mathbf{G}\mathbf{f}_c = \mathbf{F}_o \qquad \mathbf{G}^T \mathbf{V}_{po}^b = \dot{\mathbf{x}}_c \tag{13}$$

$$\mathbf{G} := \begin{bmatrix} \mathbf{A}_{g_{c_1 o}}^T \mathbf{B}_{c_1} & \cdots & \mathbf{A}_{g_{c_n o}}^T \mathbf{B}_{c_n} \end{bmatrix} \tag{14}$$

[1, Section 5.2.2, Fig. 5.15], where $\mathbf{G} \in \mathbb{R}^{3 \times \mathrm{c}}$ if $d = 2$, and $\mathbf{G} \in \mathbb{R}^{6 \times \mathrm{c}}$ if $d = 3$. As this is a self-manipulation, $\mathbf{V}_{po}^b$ is the opposite of the body velocity one would normally consider, as it is the velocity of O, attached to the world. This opposite direction comes from the more general identity, $\mathbf{V}_{po}^b = -\mathbf{Ad}_{g_{op}} \mathbf{V}_{op}^b$, [1, Lemma 2.16] (see Appendix Section F for proof), but in this case the adjoint matrix is simply identity. Therefore a self-manipulation "grasp" map is defined as,

$$\mathbf{G}_s := -\mathbf{G}, \qquad \mathbf{G}_s^T \mathbf{V}_{op}^b = \dot{\mathbf{x}}_c, \qquad \mathbf{G}_s \mathbf{f}_c = \mathbf{F}_p \tag{15}$$

where recall that $\mathbf{V}^b_{op} = \mathbf{V}^b_{wp}$ is the body velocity of P relative to any world coordinate frame, and $\mathbf{F}_p$ is the body wrench.

Next, the *hand Jacobian*, $\mathbf{J}_h$ relates infinitesimal motion at the joints, $\dot{\theta} \in T\Theta$ to twists at the contact points, $\dot{\mathbf{x}}_c \in T\mathcal{C}$, and has a dual, the pullback from contact wrenches, $\mathbf{f}_c \in T^*\mathcal{C}$ to hip torques, $\tau \in T^*\mathcal{C}$, all expressed as,

$$\mathbf{J}_h\dot{\theta} = \dot{\mathbf{x}}_c \qquad \mathbf{J}_h^T\mathbf{f}_c = \tau \tag{16}$$

[1, Section 5.5.1, Fig. 5.15], where $\mathbf{J}_h \in \mathbb{R}^{\mathrm{n}\times\mathrm{c}}$. The hand Jacobian definition carries over directly from manipulation,

$$\mathbf{J}_h := \begin{bmatrix} \mathbf{B}^T_{c_1}\mathbf{Ad}^{-1}_{g_{sc_1}}\mathbf{J}^s_{sf_1} & 0 & 0 \\ 0 & \ddots & 0 \\ 0 & 0 & \mathbf{B}^T_{c_n}\mathbf{Ad}^{-1}_{g_{sc_n}}\mathbf{J}^s_{sf_n} \end{bmatrix}.$$

Note that in the case of body contact, the hand Jacobian has a column of all zeros, that is contact wrenches at that point have no direct projection onto the joint torques (see Appendix Section B for further discussion).

Combining (13) and (16), and recalling that $\mathbf{V}^b_{op} = \mathbf{R}^T_{wp}\dot{\mathbf{x}}$, we see that as claimed in (11),

$$\mathbf{A}(\mathbf{q})\dot{\mathbf{q}} = \begin{bmatrix} -\mathbf{J}_h & \mathbf{G}_s^T\mathbf{R}^T_{pw} \end{bmatrix}\begin{bmatrix} \dot{\theta} \\ \dot{\mathbf{x}} \end{bmatrix} = \begin{bmatrix} -\mathbf{J}_h & \mathbf{G}_s^T \end{bmatrix}\begin{bmatrix} \dot{\theta} \\ \mathbf{V}^b_{op} \end{bmatrix} = \mathbf{0} \tag{17}$$

asserting that the motion of the contact frames as seen from the robot and the world agree (so long as the friction constraints hold (7)).

F. ROLLING CONTACT

Rolling contact, when the contact frame C_k is not fixed relative to either the body or object, can be treated as a simple extension to the above analysis. At each instant the velocity of the body and joints is as if the leg was a simple stick leg, with a toe at the point of contact,[4] however the evolution of the contact location is dictated by the relative geometry. The underlying contact velocity constraint is still correct, as the contact instantaneously cannot move in the constrained direction, however in general this constraint is non-holonomic [24] (i.e. there is no corresponding base constraint (8)).

Therefore in general the velocity constraint components $\mathbf{G}_s$ and $\mathbf{J}_h$ also depend on parameterized contact coordinates, η, which update as some function of the local geometry [26]. For RHex, the geometry is simple enough that no extra η parameters are needed (the rolling contact frames can be described fully by elements of $\mathbf{q}$), and so in the interest of space we direct the reader to [1, Chapter 5.6] for a full derivation (with similar notation) as well as [24]–[26]. In addition see [27], [28] for higher order considerations—for now it is sufficient to note that while the constraint, $\mathbf{A}$ (11), is the same for rolling contact as an equivalent stick leg, $\dot{\mathbf{A}}$ may not be, and so while quasi-statically both follow the same trajectory, the dynamics are different in order to account for the changing constraints. This fact is used for example in Result C.4.

[4]See the Appendix Section C for simple proof for RHex like circular legs.

G. PARAMETERIZATION OF THE CLOSED-LOOP KINEMATICS

In most of the applications settings considered below, given the c constraints (10), it is convenient to work with a local parameterization of the e = q − c dimensional manifold of remaining mobility. This amounts to the choice of an implicit function, $h : \mathcal{Y} \to \mathcal{Q}$, where $\mathcal{Y}$ is some convenient open subset of $\mathbb{R}^{\mathrm{e}}$. To simply answer certain questions about the robot motion in terms of particular components of $\mathbf{q}$, it is convenient to identify $\mathcal{Y}$ with a problem-specific Euclidean submanifold of our generalized coordinates, i.e. $\mathcal{Y} := \psi(\mathcal{Q})$, where, in coordinates, ψ is some fixed linear combination of the components of $\mathbf{q}$ corresponding to the directions of interest in the problem (and often a projection whose matrix representation is a subcollection of columns from the identify matrix). The tangent map, $\mathbf{Y} := D\psi$, $\mathbf{Y} \in \mathbb{R}^{\mathrm{q}\times\mathrm{e}}$, results in a combined constraint equation,

$$\begin{bmatrix} \mathbf{A} & 0 \\ \mathbf{Y} & -\mathbf{Id}_{\mathrm{e}} \end{bmatrix}\begin{bmatrix} \dot{\mathbf{q}} \\ \dot{\mathbf{y}} \end{bmatrix} = 0$$

such that the associated implicit function (split into hand and object components),

$$\mathbf{h}_h(\mathbf{y}) = \theta, \qquad \mathbf{h}_o(\mathbf{y}) = \mathbf{x}, \qquad \mathbf{h} = (\mathbf{h}_h, \mathbf{h}_o) : \mathcal{Y} \to \mathcal{Q} \tag{18}$$

is a local immersion—i.e., its Jacobian maps,

$$\dot{\theta} = \mathbf{H}_h\dot{\mathbf{y}}, \qquad \dot{\mathbf{x}} = \mathbf{H}_o\dot{\mathbf{y}}, \qquad \mathbf{H} := D_{\mathbf{y}}\mathbf{h} \tag{19}$$

$$\mathbf{H} = \begin{bmatrix} \mathbf{A} \\ \mathbf{Y} \end{bmatrix}^{-1}\begin{bmatrix} 0 \\ \mathbf{Id}_{\mathrm{e}} \end{bmatrix} \tag{20}$$

is full rank (never passing through the origin) in both tangent spaces (for some local region in $\mathcal{Y}$). In this paper we assume that such a parameterization exists. The matrix inverted in (20) is dimension q×q, and invertible except at singularities in the kinematics or parameterization. Note that $\mathbf{H}_h$ can be thought of as the instantaneous gear ratios for n independent motor shafts coupled rigidly to an external output load with e DOF.

This implicit function is used to show that the change of basis in Section IV-A is a good approximation, and again in Section IV-B.3 that $\mathbf{H}_o$ can be used to control the pitching rate of the robot.

H. QUASI-STATIC FORCES AND TORQUES

The wrench due to the gravitational potential field, $\mathbf{F}_g$, is derived from the height $\zeta : \mathcal{G}_p \to \mathbb{R}$ in that potential field and, at static equilibrium, it is exactly balanced by the contact forces through the grasp map (13),

$$\mathbf{G}_s\mathbf{f}_c = -\mathbf{F}_g. \tag{21}$$

If the number of DOF in the closed-chain analysis, e, is less than the number of motors, n, there is some ''internal'' force components, which lies in the subspace [1, Definition 5.3],

$$\ker(\mathbf{G}_s) = \mathrm{Im}(\mathbf{f}_N) := \left\{ \sum_{i=1}^{\mathrm{a}} \alpha_i\mathbf{f}_{Ni} | \alpha_i \in \mathbb{R} \right\} \tag{22}$$

that forms the homogeneous solution, i.e. contact wrenches that are *internal* in that they can perform no work on the object, where a := n − e.

To invert (21) and determine the contact forces required to balance the external wrench, torque constraints[5] of the form $\mathbf{t}_i^T \tau = 0, i \leq$ a must be imposed upon the hip joint torque vector, $\tau \in T^*\Theta$, (16). Pulling back through the infinitesimal kinematics, this now constrains the contact wrench magnitude vector $\mathbf{f}_c \in T^*\mathcal{C}$ leading to a unique solution of the full rank augmented version of (21) taking the form,

$$\mathbf{t}^T \mathbf{J}_h^T \mathbf{f}_c = 0, \qquad \mathbf{f}_p := -\begin{bmatrix} \mathbf{G}_s \\ \mathbf{t}^T \mathbf{J}_h^T \end{bmatrix}^{-1} \begin{bmatrix} \mathbf{F}_g \\ 0 \end{bmatrix}. \tag{23}$$

Thus the overall vector of contact wrench magnitudes is,

$$\mathbf{f}_c = \mathbf{f}_p + \sum_i \alpha_i \mathbf{f}_{Ni}$$

and the internal and external components may be projected back into motor torques through (16).

These quasi-static internal and external forces are the key to the reactive standing behavior in Section IV-A, and calculating the torque requirement in the pitching sensor sweep (Section IV-B.2).

I. DYNAMICS

This section derives a Lagrangian formulation for the robot dynamics in terms of some local coordinates, arriving at a relationship between $\mathbf{q}, \dot{\mathbf{q}}$, and $\ddot{\mathbf{q}}$ in (33). We allow for the option of having massless legs, and so expressions of the dynamics cannot involve directly inverting the mass matrix.

If the body of the robot has mass m_b and inertia I_b, and each leg segment may have mass m_{l_i} and inertia I_{l_i}, then observe that the total kinetic energy is,[6]

$$T = \frac{1}{2}\begin{bmatrix}\dot{\theta}^T & \mathbf{V}_{op}^{bT}\end{bmatrix} \widehat{\mathbf{M}} \begin{bmatrix}\dot{\theta} \\ \mathbf{V}_{op}^{b}\end{bmatrix} = \frac{1}{2}\dot{\mathbf{q}}^T \overline{\mathbf{M}} \dot{\mathbf{q}} \tag{24}$$

$$\widehat{\mathbf{M}} := \begin{bmatrix} \sum_i \mathbf{J}_{pl_i}^{bT} \mathbf{M}_{l_i} \mathbf{J}_{pl_i}^{b} & \sum_i \mathbf{J}_{pl_i}^{bT} \mathbf{M}_{l_i} \mathbf{Ad}_{g_{pl_i}^{-1}} \\ \sum_i \mathbf{Ad}_{g_{pl_i}^{-1}}^T \mathbf{M}_{l_i} \mathbf{J}_{pl_i}^{b} & \mathbf{M}_b + \sum_i \mathbf{Ad}_{g_{pl_i}^{-1}}^T \mathbf{M}_{l_i} \mathbf{Ad}_{g_{pl_i}^{-1}} \end{bmatrix} \tag{25}$$

$$\mathbf{M}_i := \begin{bmatrix} m_i \mathbf{Id}_d & 0 \\ 0 & I_i \end{bmatrix}, \quad \overline{\mathbf{M}} := \begin{bmatrix} \mathbf{Id}_n & 0 \\ 0 & \mathbf{R}_{wp} \end{bmatrix} \widehat{\mathbf{M}} \begin{bmatrix} \mathbf{Id}_n & 0 \\ 0 & \mathbf{R}_{wp}^T \end{bmatrix} \tag{26}$$

(see Appendix Section D for full derivation) where recall that $\mathbf{J}_{pl_i}^b \dot{\theta} = \mathbf{V}_{pl_i}^b$.

The potential energy depends on the world-referenced height of the body in the gravitational field, $\zeta_o(\mathbf{x})$, and the configuration-dependent height of each link relative to the body, $\zeta_l(\theta, \phi)$,

$$V(\mathbf{q}) = m_b g \zeta_o(\mathbf{x}) + \sum_{l=1}^{n} m_l g(\zeta_o(\mathbf{x}) + \zeta_l(\theta, \phi)). \tag{27}$$

[5]Alternatively a "no internal force" constraint may be encoded as $\mathbf{f}_N^T \mathbf{f}_c = 0$ [2], however in general we allow some internal force to achieve some other goal, such as no internal torque.

[6]This "self-manipulation" inertia tensor (25) is much simpler when the legs are taken to be massless, $\mathbf{M}_{l_i} = 0 \Rightarrow \widehat{\mathbf{M}} = \left[\begin{smallmatrix} 0 & 0 \\ 0 & \mathbf{M}_b \end{smallmatrix}\right]$, and quite different than in manipulation, $\widehat{\mathbf{M}} = \left[\begin{smallmatrix} \sum \mathbf{J}^T \mathbf{M}_i \mathbf{J} & 0 \\ 0 & \mathbf{M}_b \end{smallmatrix}\right]$, (as in [1, Eqn. 6.24]), where the extra terms in (25) arise from the coupling inherent in self-manipulation.

Using these statements of the kinetic and potential energy, and applying Lagrange's equations [1, Eqn. 6.4], [41, Sec. 5.1],

$$L(\mathbf{q}, \dot{\mathbf{q}}) = \frac{1}{2}\dot{\mathbf{q}}^T \overline{\mathbf{M}}(\theta, \phi)\dot{\mathbf{q}} - V(\mathbf{q}) = \frac{1}{2}\sum_{i,j=1}^{q} \overline{M}_{ij}\dot{q}_i\dot{q}_j - V(\mathbf{q}) \tag{28}$$

$$0 = \frac{d}{dt}\frac{\partial L}{\partial \dot{q}_i} - \frac{\partial L}{\partial q_i} + \mathbf{A}^T\lambda - \Upsilon$$

$$\frac{d}{dt}\frac{\partial L}{\partial \dot{q}_i} = \frac{d}{dt}\left(\sum_{i,j=1}^{q} \overline{M}_{ij}\dot{q}_j\right) = \sum_{i,j=1}^{q}\left(\overline{M}_{ij}\ddot{q}_j + \dot{\overline{M}}_{ij}\dot{q}_j\right)$$

$$\frac{\partial L}{\partial q_i} = \frac{1}{2}\sum_{j,k=1}^{q} \frac{\partial \overline{M}_{kj}}{\partial q_i}\dot{q}_k\dot{q}_j - \frac{\partial V}{\partial q_i}. \tag{29}$$

The Coriolis terms may be grouped in the usual way,[7]

$$\overline{C}_{ij} = \frac{1}{2}\sum_{k=1}^{q}\left(\frac{\partial \overline{M}_{ij}}{\partial q_k} + \frac{\partial \overline{M}_{ik}}{\partial q_j} - \frac{\partial \overline{M}_{kj}}{\partial q_i}\right)\dot{q}_k \tag{30}$$

and the nonlinear (gravitational) and applied forces are,

$$\overline{N}_i(\theta, \phi) = \frac{\partial V}{\partial q_i}, \qquad \Upsilon(\tau) = \begin{bmatrix} \tau \\ \mathbf{0} \end{bmatrix} \tag{31}$$

where $\overline{\mathbf{N}}$ depends only on θ and ϕ as the force due to gravity is position independent. Note that damping may also be modeled with $\overline{\mathbf{N}}$, in which case it depends on $\dot{\mathbf{q}}$.

The constraint forces, $\mathbf{A}^T\lambda$, arise from the closed-loop constraint (11), and the contact force magnitudes must satisfy the friction constraint (7), $\mathbf{U}(\lambda) \geq 0$.

Rearranging (29) into the familiar form, where note that $\mathbf{A}$ is the only term that varies with contact mode,

$$\overline{\mathbf{M}}(\theta, \phi)\ddot{\mathbf{q}} + \overline{\mathbf{C}}(\theta, \phi, \dot{\mathbf{q}})\dot{\mathbf{q}} + \overline{\mathbf{N}}(\theta, \phi) + \mathbf{A}^T(\mathbf{q})\lambda = \Upsilon(\tau) \tag{32}$$

the dynamics and the constraints may be combined in a few different ways to solve for $\ddot{\mathbf{q}}$ and λ, here we choose,

$$\begin{bmatrix}\ddot{\mathbf{q}} \\ \lambda\end{bmatrix} = \underbrace{\begin{bmatrix}\overline{\mathbf{M}} & \mathbf{A}^T \\ \mathbf{A} & 0\end{bmatrix}^{-1}\begin{bmatrix}\Upsilon - \overline{\mathbf{N}} \\ 0\end{bmatrix}}_{\mathbf{E}(\theta,\phi,\tau)} - \underbrace{\begin{bmatrix}\overline{\mathbf{M}} & \mathbf{A}^T \\ \mathbf{A} & 0\end{bmatrix}^{-1}\begin{bmatrix}\overline{\mathbf{C}} \\ \dot{\mathbf{A}}\end{bmatrix}}_{\mathbf{D}(\theta,\phi,\dot{\mathbf{q}})}\dot{\mathbf{q}} \tag{33}$$

where we assume that the inverted matrix in (33) is nonsingular even if $\overline{\mathbf{M}}$ is not (see Appendix Section D).

This formulation of the dynamics is sufficient to determine, for example, that the front leg always lifts off the ground before the rear leg in a symmetric leap (Section IV-C.1). However it is convenient to use the parameterization of Section II-G to separate the free dynamics from the constraint forces, as shown in the next section.

J. REDUCED DYNAMICS

Instead of working with the complete dynamics we can instead consider only the e free Lagrangian variables in $\mathbf{y}$, as introduced above. In this case the dynamics are,

[7]The $\overline{\mathbf{C}}$ matrix does not have any particular block diagonal structure as was the case in a manipulation problem [1, Eqn. 6.24]. If the legs are considered massless then $\overline{\mathbf{C}}$ may all be zeros, depending on parameterization.

$$\tilde{\mathbf{M}}(\mathbf{q})\ddot{\mathbf{y}} + \tilde{\mathbf{C}}(\mathbf{q}, \mathbf{H}(\mathbf{q})\dot{\mathbf{y}})\dot{\mathbf{y}} + \tilde{\mathbf{N}}(\mathbf{q}) = \tilde{\Upsilon} \tag{34}$$

$$\ddot{\mathbf{y}} = \underbrace{\tilde{\mathbf{M}}^{-1}(\mathbf{q})\left(\tilde{\Upsilon} - \tilde{\mathbf{N}}(\mathbf{q})\right)}_{\tilde{\mathbf{E}}(\mathbf{q})} - \underbrace{\tilde{\mathbf{M}}^{-1}(\mathbf{q})\tilde{\mathbf{C}}(\mathbf{q}, \mathbf{H}(\mathbf{q})\dot{\mathbf{y}})}_{\tilde{\mathbf{D}}(\mathbf{q},\dot{\mathbf{y}})}\dot{\mathbf{y}} \tag{35}$$

where,

$$\tilde{\mathbf{M}} := \mathbf{H}^T\overline{\mathbf{M}}\mathbf{H}, \qquad \tilde{\mathbf{C}} := \mathbf{H}^T\overline{\mathbf{C}}\mathbf{H} + \mathbf{H}^T\overline{\mathbf{M}}\dot{\mathbf{H}} \tag{36}$$

$$\tilde{\mathbf{N}} := \mathbf{H}^T\overline{\mathbf{N}}, \qquad \tilde{\Upsilon} := \mathbf{H}^T\Upsilon, \tag{37}$$

(see Appendix Section E for derivation). Note that while the base constraint is a function of the initial conditions ($\hat{\mathbf{x}}_c$), the Jacobian constraint is not, and so any analysis that holds across any initial conditions needs the full $\mathbf{q}$. Furthermore in general rolling contact requires non-holonomic constraints, and so $\mathbf{h}$ may not exist. Therefore we have left $\mathbf{q}$ in explicitly in (35) and write out the reduced dynamics in terms of both the reduced variables, $\mathbf{y}$, and original variables, $\mathbf{q}$, (although $\mathbf{h}(\mathbf{y})$ may be substituted for $\mathbf{q}$ when possible).

To recover the original configuration space accelerations and Lagrange multipliers,

$$\ddot{\mathbf{q}} = \mathbf{H}\ddot{\mathbf{y}} + \dot{\mathbf{H}}\dot{\mathbf{y}}. \tag{38}$$

$$\lambda = \underbrace{\mathbf{A}^*(\Upsilon - \overline{\mathbf{N}})}_{\tilde{\mathbf{E}}_\lambda(\mathbf{q})} - \underbrace{\mathbf{A}^*(\overline{\mathbf{M}}\dot{\mathbf{H}} + \overline{\mathbf{C}}\mathbf{H})}_{\tilde{\mathbf{D}}_\lambda(\mathbf{q},\dot{\mathbf{y}})}\dot{\mathbf{y}} \tag{39}$$

where $\mathbf{A}^*$, a left inverse of $\mathbf{A}$, is chosen to also satisfy $\mathbf{A}^*\overline{\mathbf{M}}\mathbf{H} = \mathbf{0}$, that is,

$$\begin{bmatrix} \mathbf{A}^* \\ (\overline{\mathbf{M}}\mathbf{H})^* \end{bmatrix} := \begin{bmatrix} \mathbf{A}^T & \overline{\mathbf{M}}\mathbf{H} \end{bmatrix}^{-1}$$

$$\Rightarrow \mathbf{A}^*\mathbf{A}^T = \mathbf{Id}_c, \quad \mathbf{A}^*\overline{\mathbf{M}}\mathbf{H} = \mathbf{0} \tag{40}$$

(see Appendix Section E for derivation).

These reduced dynamics lead to, for example, a simple proof that stubbing the toe at the end of stance in pronk is beneficial to the robot's pitch, as described in Section IV-C.3.

K. SUMMARY OF ASSUMPTIONS

For convenience, the assumptions made by the self-manipulation framework just presented are summarized as follows:

A.1) There is a distinguished (pre-selected) rigid body on the robot with a frame, P, attached at the COM.
A.2) There is an inertial world frame, W, at some (possibly unknown) fixed location, and at each instant is rigidly connected to a frame, O, co-located at P.
A.3) The robot is in contact with the world at some finite number of points, C_k, and the set of all possible contact points is known (albeit, in general, not their location).
A.4) The combined mass matrix $\overline{\mathbf{M}}$ does not need to be full rank (i.e. there may be massless limbs), however the reduced mass matrix, $\tilde{\mathbf{M}}$, is (i.e. any massless links are constrained such that the overall system motion is well defined).
A.5) Some choice of generalized coordinates, i.e., a non-singular minimal parameterization of the free motion, $\mathbf{y}$, is available in any mode of interest.

Furthermore the following assumptions are made in this paper, but not fundamental to the structure of the framework,

B.1) There are no elastic or compliant components.
B.2) Any damping or air resistance is negligible.

Some additional assumptions are made when this general framework is instantiated in the next section.

III. SELF-MANIPULATION FOR RHex

A. MODEL PARAMETERS

When RHex uses pairs of contralateral legs in phase on level ground, it is very effectively anchored to the sagittal plane, and so here we develop a planar model for RHex ($d := 2$), with only two legs modeled, each with one joint ($n := 2$, $q = 5$), as shown in Fig. 3. In addition the body is allowed to contact the ground at up to two locations (front and rear), so that $k \leq 4$. The rubber treads on the toes have a relatively high coefficient of friction (especially on rough outdoor terrain) that we assume always resists tangential (sliding) motion, while the hard shell of RHex's body has a very low coefficient of friction and so we assume that the body always is able to slide. There are thus 2 contact wrenches at each toe and 1 at the front and rear of the robot, implying that $c \leq 6$. We do not assume that the robot is endowed with any exteroceptive sensors, and as such must assume instead that the robot is on flat level ground, and so the contact normals are aligned with gravity.

The location and orientation of the various frames are shown in Fig. 3. In the palm frame, let the $+\mathbf{x}$ axis be aligned with the robot, $+\mathbf{z}$ in the "downward" direction from the robot, and thus $+\mathbf{y}$ exiting the page (this is a standard "North, East, Down" orientation). Hip i (S_i) is located ℓ_i away from the P frame along the positive $\mathbf{x}$ direction, and the leg length is ρ_i putting the F_i frame at ρ_i along the positive $\mathbf{z}$ direction from M_i, thus,

$$\mathbf{g}_{pc_1}(\theta, \phi) := [\ \ell_1 - \rho_1 \sin\theta_1,\ \rho_1 \cos\theta_1,\ -\phi]^T$$
$$\mathbf{g}_{pc_2}(\theta, \phi) := [-\ell_2 - \rho_2 \sin\theta_2,\ \rho_2 \cos\theta_2,\ -\phi]^T$$

when the leg is supported on its toe ($0 \leq \theta_i - \phi < \pi$, as with leg 2 in Fig. 3). While the leg is in rolling contact (as with leg 1 in Fig. 3),

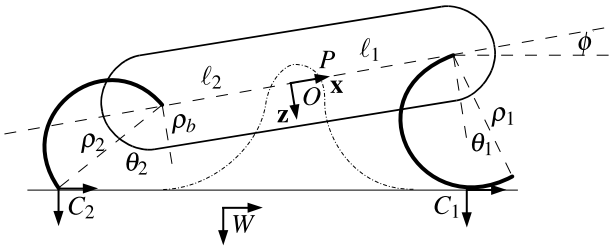

FIGURE 3. Coordinate frames and key dimensions for RHex under the self-manipulation formulation.

TABLE 2. Physical quantities used in the RHex model. Note that m_l, I_l, and τ_s are doubled in practice as contra-lateral legs are used in parallel in this paper, though all but the last behavior assume massless legs.

Symbol	Value	Definition
m_b	7.15 kg	Body Mass
I_b	0.15 kg·m^2	Body Inertia
m_l	0.063 kg	Leg Mass
I_l	0.00046 kg·m^2	Leg Inertia
ℓ_1, ℓ_2	20.5 cm	Body-Hip Length
ρ_1, ρ_2	17 cm	Leg Length
ρ_b	5 cm	Body Radius
τ_s	15 N·m	Saturated Maximum Torque

$$\mathbf{g}_{pc_1}(\theta,\phi) := \Big[\ \ell_1 - \frac{\rho_1}{2}(\sin\theta_1 + \sin\phi),\ \frac{\rho_1}{2}(\cos\theta_1 + \cos\phi),\ -\phi\Big]^T$$
$$\mathbf{g}_{pc_2}(\theta,\phi) := \Big[-\ell_2 - \frac{\rho_2}{2}(\sin\theta_2 + \sin\phi),\ \frac{\rho_2}{2}(\cos\theta_2 + \cos\phi),\ -\phi\Big]^T.$$

The body has semi-circular ends with radius ρ_b about the hips and so the two potential body contact points are,

$$\mathbf{g}_{pc_3}(\theta,\phi) := [\ \ell_1 - \rho_b\sin\phi,\ \rho_b\cos\phi,\ -\phi]^T$$
$$\mathbf{g}_{pc_4}(\theta,\phi) := [-\ell_2 - \rho_b\sin\phi,\ \rho_b\cos\phi,\ -\phi]^T.$$

The body pitch is $\phi = 0$ when the robot is horizontal and a positive pitch when hip 1 is higher than hip 2. The leg angles are measured as θ_1 and θ_2 in the clockwise direction from the body $+\mathbf{z}$ direction. In Fig. 3, $\theta_1 < 0, \theta_2 > 0, \phi > 0$. Physical values used, including lengths and masses, are summarized in Table 2.

B. RHex KINEMATICS

The definitions of the previous subsection completely describe the kinematics and dynamics of the robot in any contact configuration. A full list of the resulting matrix formulation of the kinematics and dynamics is included in the Appendix Section G, while here we only look at the base constraint and explore the quasi-static state space.

From Section II-D, the base kinematic constraint is defined by composing the inverse of the specified maps for $\mathbf{g}_{pc_k}$ with the body coordinates, $\mathbf{x}$, which for stick legs ($0 \le \theta_i - \phi < \pi$),

$$\begin{aligned}\mathbf{a}_k(\mathbf{q}) &= \pi(\mathbf{g}_{c_k w}(\mathbf{q})) - \hat{\mathbf{x}}_{c_k}, \quad k \in 1,2\\ &= \begin{bmatrix} -x - \ell_k\cos(\phi) + \rho_k\sin(\theta_k - \phi) \\ -z + \ell_k\sin(\phi) - \rho_k\cos(\theta_k - \phi)\end{bmatrix} - \begin{bmatrix}\hat{x}_{c_k}\\ \hat{z}_{c_k}\end{bmatrix}\end{aligned} \tag{41}$$

while for rolling contact ($-\pi \le \theta_i - \phi < 0$),

$$\begin{aligned}\mathbf{a}_k(\mathbf{q}) &= \pi(\mathbf{g}_{c_k w}(\mathbf{q})) - \hat{\mathbf{x}}_{c_k}, \quad k \in 1,2\\ &= \begin{bmatrix} -x - \ell_k\cos(\phi) + \frac{\rho_k}{2}\sin(\theta_k - \phi) \\ -z + \ell_k\sin(\phi) - \frac{\rho_k}{2}(1 - \cos(\theta_k - \phi))\end{bmatrix} - \begin{bmatrix}\hat{x}_{c_k}\\ \hat{z}_{c_k}\end{bmatrix}.\end{aligned} \tag{42}$$

Similarly for the body contact, the base kinematic map is,

$$\begin{aligned}\mathbf{a}_k(\mathbf{q}) &= \pi_z(\mathbf{g}_{c_k w}(\mathbf{q})) - \hat{\mathbf{x}}_{c_k}, \quad k \in 3,4\\ &= \big[-z + \ell_k\sin(\phi) - \rho_b\big] - \big[\hat{z}_{c_k}\big]\end{aligned} \tag{43}$$

which is the equivalent of setting $\theta_k = \phi$.

As introduced in Section II-C, the active contact constraints can be found by checking the height of each potential contact frame, $\zeta_{c_k}(\mathbf{x})$. If however the robot does not know its exact place in the world ($\pi(\mathbf{x})$), the contact condition can still be found by relying on the assumptions of flat level ground and quasi-static operation. First since the robot is quasi-static, choose the world reference frame to be $W \equiv O$, and so $\pi(\mathbf{x}) = 0$. In this case the active contact points are simply those that are farthest from the body in their $\mathbf{z}$ direction, which recall is always non-positive by convention,

$$\pi_z(\mathbf{g}_{c_k o}) < \pi_z(\mathbf{g}_{c_i o}), \quad \forall k \in \mathcal{K}, i \notin \mathcal{K}.$$

To consider the difference between rolling contact (on the rounded part of the half circle leg) and point contact (on the toe of the leg) a further condition is needed that specifies which part of the leg are rounded. In particular, the leg presents the rounded half of its shape when $-\pi < \theta_i - \phi < 0$ (as opposed to e.g. [42] which is rounded on the other half).

Once contact mode is determined, pitch is an implicit function of the equality of the constraint (10), $0 \equiv \mathbf{a}_{c_k}(\mathbf{q})$. As before, take $\pi(\mathbf{x}) \equiv 0$, and so,

$$\begin{aligned}&\pi_z(\mathbf{a}_{c_i}) - \pi_z(\mathbf{a}_{c_j}) \equiv 0, \quad \forall i,j \in \mathcal{K}\\ &\pi_z(\mathbf{g}_{c_i o}) \equiv \pi_z(\mathbf{g}_{c_j o})\end{aligned} \tag{44}$$

from which we can locally derive the body pitch as an implicit function of the joint angles. These conditions are combined

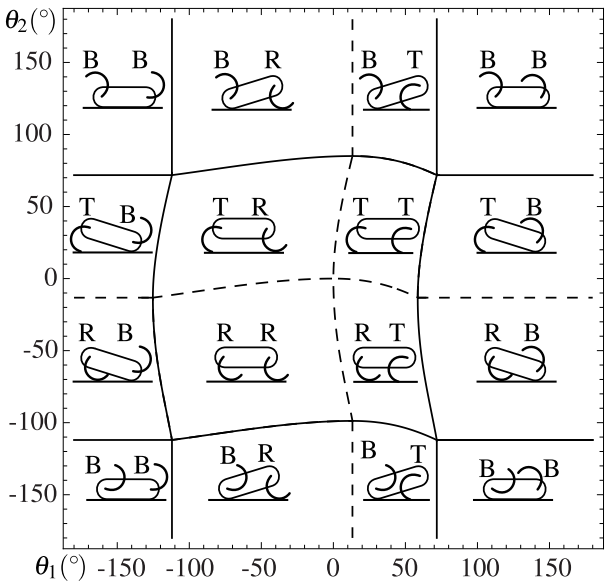

FIGURE 4. Quasi-static contact modes over the entire state space of joint angles ($\Theta \approx \mathbb{T}^2$). Each region is distinguished by front and rear contact conditions that can be Body, Rolling, or Toe contact, as indicated by the respective letter.

to create Fig. 4, which shows the various quasi-static contact conditions across the entire joint space, Θ.

C. ASSUMPTIONS FOR RHex

As a summary, the following assumptions, in addition to those listed in Section II-K, are made about the RHex model,

C.1) RHex is anchored to the sagittal plane by using contralateral legs together, and so $d = 2$.
C.2) The middle legs are not used, and so $n = 2$.
C.3) The body can contact in up to two locations but has a low coefficient of friction that never resists tangential friction forces.
C.4) The rubber toes have a high coefficient of friction and therefore always resist tangential forces (as the surface normal and frictional coefficients for novel terrain is unknown—if they are assumed to be known then the friction cone could be checked with (7)).
C.5) The robot is on flat level ground (C_k aligned with W, assumed everywhere except Section IV-A).
C.6) The legs are massless ($m_l \equiv 0$, $I_l \equiv 0$, assumed everywhere except Section IV-C.5).

Furthermore the following simplifying assumptions are made in some of the following behaviors as marked,

D.1) The robot is near a nominally standing posture, i.e. the legs are "under" the robot, $\theta_k \in \mathcal{U} := [-30°, 30°]$, and the robot is close to level, $\phi \in [-10°, 10°]$.
D.2) The robot is symmetric ($\ell_1 \equiv \ell_2 := \ell$, $\rho_1 \equiv \rho_2 := \rho$, implicitly assumed for numerical calculations based on Table 2).
D.3) The robot is a point mass ($I_b \equiv 0$).

IV. BEHAVIORS

A. REACTIVE STANDING

In this section we document a quasi-static RHex standing controller that delivers up to a 90% reduction in power use relative to an open-loop stand on unmodeled rough terrain [13]. The scheme is extraordinarily simple: the controller seeks simultaneously to reduce the variance of joint torques around their mean (right side of Fig. 5), while fighting to "lean up" against the mean load (left side of Fig. 5). The self-manipulation model is needed to formalize these insights and establish the correctness of the controller.

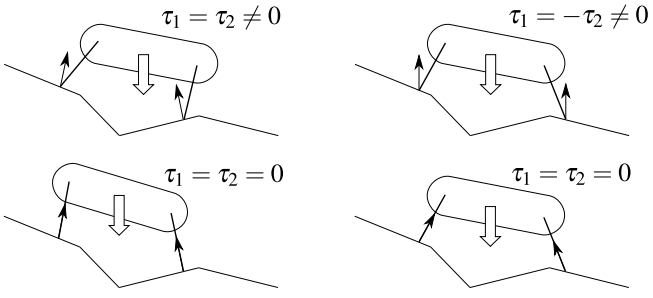

FIGURE 5. Two examples of how the balancing stand works, noting the relationship between motor torques. On the left, start and end conditions for fighting an external force, on the right start and end conditions for relaxing an internal force.

This notion of fighting an external force and relaxing the internal force has been used before on legged robots, usually without stating it in this way. For example, prior work on RHex pushes the body uphill to be centered over the legs while climbing steep terrain [43], and separately regulate individual leg torques such that no one leg pushes harder than the rest [44]. These ideas were further developed on RiSE [45], [46] whose reactive gait phase adjustments were designed to balance forces within and between the sides. Similar internal force management strategies have been suggested on quadrupeds [47] and highly articulated bipeds [48], though without a proof of convergence.

To analyze this behavior, Section IV-A.1 decomposes the motor cost into average and difference terms, ϵ and δ, and derive the quasi-static torques necessary to fight external (gravity) and any internal (legs fighting) wrenches. The key to this decomposition is to apply the closed-loop constraint to find the internal and external forces at the toes (Section II-H), and projecting that back into motor torques (Section II-E). Section IV-A.2 sets up the controller summarized in Fig. 5, in part by using an approximation to the closed-loop velocity constraint (Section II-G). Section IV-A.3 brings these parts all together and show convergence of the controller. This entire behavior is analyzed using stick legs with point contact, but as Section II-F has shown, the free motion of rolling contact is the same as that of a stick leg with appropriate radius, and so by showing Lyapunov convergence for any angle and any leg lengths (within appropriate bounds), the rolling contact can be ignored. Note that this proof does not rely on Assumption C.5 but instead simply uses Assumptions C.4 and D.1. Finally Section IV-A.4 tests this controller on a variety of indoor and outdoor terrain, with results documented in Table 3.

1) PROBLEM SETUP

For this problem we are trying to minimize the thermal cost needed to stand, which is proportional to the square of current (which in turn is proportional to torque). A natural goal to set is $\Pi := \frac{1}{2}\left(\tau_1^2 + \tau_2^2\right)$. A key insight is to break apart the functional form of $\Pi = \epsilon(\tau_1, \tau_2) + \delta(\tau_1, \tau_2)$, where $\epsilon(\tau_1, \tau_2) := \tau_m^2$ is the squared mean torque, and $\delta(\tau_1, \tau_2) := \tau_d^2$, is the squared difference in torques,

$$\begin{bmatrix} \tau_m \\ \tau_d \end{bmatrix} := \mathbf{T}\tau \qquad \mathbf{T} := \begin{bmatrix} \mathbf{t}_m^T \\ \mathbf{t}_d^T \end{bmatrix} = \frac{1}{2}\begin{bmatrix} 1 & 1 \\ 1 & -1 \end{bmatrix} \tag{45}$$

and analogously $[\theta_m \quad \theta_d]^T := \mathbf{T}\theta$. Section IV-A.3 shows that ϵ captures the cost due to gravity while δ captures the cost due to internal forces, and more importantly the proposed controller drives both costs to zero.

Similarly we may choose to parameterize the implicit function associated with the closed-loop constraint by the average velocity, with $y \equiv \theta_m = \mathbf{t}_m^T\theta$, i.e. $\dot{y} = \mathbf{Y}\dot{\mathbf{q}} := \frac{1}{2}[1\ 1\ 0\ 0\ 0]\dot{\mathbf{q}}$. This choice is motivated by the observation that motion has equal cost in both motors, though selection of $y \equiv \theta_1$ or

$y \equiv \theta_2$ also works well. The Jacobian of the associated implicit function (19) on some open neighborhood of the origin, $\mathcal{U} \subset \mathbb{R}$, is,

$$\mathbf{H}_h := D_{\theta_m}\mathbf{h}_h = \frac{2}{\gamma_1+\gamma_2}\begin{bmatrix}\gamma_1\\ \gamma_2\end{bmatrix} \tag{46}$$

$$\gamma_i := (\ell_1+\ell_2)\rho_j\cos\theta_j + \rho_1\rho_2\sin(\theta_2-\theta_1), \quad j = 3-i \tag{47}$$

and is full rank (never passing through the origin) in both tangent spaces as the "gear ratios," γ_k, are always positive and nearly equal (bounded numerically by $0.83 \leq \gamma_1/\gamma_2 \leq 1.19$ under Assumption D.1 in [13]).

The "internal" component of the forces at the toes lies in the subspace defined by (22), which form the homogeneous solution, i.e. toe forces that are *internal* in that they can perform no work on the object. To specify a particular solution, apply (23) with $\mathbf{t}^T \equiv \mathbf{t}_d^T$. This choice of particular solution, depicted in the lower sketches of Fig. 5, corresponds to toe forces that cancel gravity with the "right amount" of internal force, here defined by the difference condition.

The torque produced by these toe forces is given by the hand Jacobian, $\mathbf{J}_h^T$, as in (16). It is convenient to work in a new basis for the joint-space torques, $\tau \in T^*\Theta$, given by the scaled rotational transformation $\mathbf{T}$ into the mean and difference of the torques as defined in (45). The torque implication of the particular solution ($\alpha = 0$) is,

$$\begin{bmatrix}\tau_m\\ \tau_d\end{bmatrix}_p := \mathbf{T}\mathbf{J}_h^T\mathbf{f}_p = -m_b g\rho_1\rho_2 \times \frac{\ell_1\cos\theta_1\sin(\theta_2-\phi)+\ell_2\cos\theta_2\sin(\theta_1-\phi)}{\gamma_1+\gamma_2}\begin{bmatrix}1\\ 0\end{bmatrix} \tag{48}$$

where $\tau_{d,p} = 0$ because the particular solution has no component in the $\mathbf{t}_d^T$ direction (23). Therefore all of the virtual work against gravity must show up in $\tau_{m,p}$, so that $\tau_{m,p} = \frac{1}{2}\mathbf{F}_g^T\mathbf{H}_o = \frac{1}{2}m_b g D\zeta \circ D\mathbf{h}_o$ (see [13] for proof).

The torque projection of the homogeneous solution is,

$$\begin{bmatrix}\tau_m\\ \tau_d\end{bmatrix}_h := \alpha\mathbf{T}\mathbf{J}_h^T\mathbf{f}_N = \frac{\alpha}{2}\begin{bmatrix}\gamma_2-\gamma_1\\ \gamma_2+\gamma_1\end{bmatrix}. \tag{49}$$

Here there is not an exact decomposition—we would like $\tau_{m,h}$ to be zero so that τ_m is exactly $\tau_{m,p}$. However we have observed (in (47) and related discussion) that $\gamma_1 \approx \gamma_2$, and in any case if our controller is successful we can achieve this by simply canceling the internal force magnitude, α. Having derived an expression for the various torque components in (48)–(49), we can now apply a controller to this system and observe the effect on the component cost functions, ϵ and δ.

2) CONTROLLER DESIGN

In this section, we show how direct current readings at the hips yield intrinsic sensors that approximate the gradient of two costs, ϵ and δ, eliminating all need to know or compute the exact kinematics online. The change of basis in torque space, $\mathbf{T}$, allows the robot to use these sum and difference torque measurements to closely approximate the gradient of its power-use cost function.

Because the motor controller is highly overdamped and rate limited we adopt "generalized damper" mechanics and model the motor as velocity controlled in general, $\dot\theta = \kappa_p\tilde\theta$, for some command $\tilde\theta \in T\Theta$. To guarantee that the system remains quasi-static, this command is rate limited to ensure $\tilde\theta \leq \kappa_\sigma$. However the motion is constrained by the closed-loop condition (12), and so the constrained motion is approximately,

$$\dot\theta_m = \kappa_p\tilde\theta_m \tag{50}$$

$$\dot\theta_d = 0 \tag{51}$$

since the system can move freely in approximately the θ_m direction (exactly, in the $\mathbf{H}_h$ (46) direction). In contrast, in the approximate θ_d direction (exactly, along infinitesimal motions orthogonal to $\mathbf{H}_h$), motion is locked, hence generated torque must increase as,

$$\dot\tau_d = \kappa_t\tilde\theta_d, \tag{52}$$

i.e. any differentially applied command increases the torque as the system cannot move in that direction.

Again, we emphasize that this locked leg assumption is merely an approximation (as $\partial\theta_d/\partial\theta_m$ is small), but no matter how large the shift, so long as $\gamma > 0$ for all angles, i.e. the sign of the direction of motion is correct, we can simply allow the internal force controller to compensate for this "disturbance" in θ_d as the robot moves.[8] Moreover this misalignment between the approximate and true parameterization of the free motion does not affect the zero point—in either case the zero has $\tau_1 = \tau_2 = 0$ and so the controller converges to the correct place, even if it does not take the "most direct" route.

3) INTERNAL AND EXTERNAL COST

Note that the internal cost, $\delta = \tau_d^2 = \alpha^2(\gamma_1+\gamma_2)^2/4$ (49), vanishes if $\alpha = 0$. Therefore since the particular solution makes no contribution to τ_d (48), based on our actuator model (51)–(52), it is straightforward to reduce δ by asserting a control policy, $\tilde\theta_d := -\kappa_d\tau_d$, resulting in,

$$\dot\delta = 2\tau_d\dot\tau_d = \begin{cases}-2\kappa_d\kappa_t\tau_d^2 & |\tilde\theta_d| \leq \kappa_\sigma\\ -2\kappa_d\kappa_t\kappa_\sigma|\tau_d| & |\tilde\theta_d| > \kappa_\sigma.\end{cases} \tag{53}$$

Thus the positive definite function, δ, has a negative definite derivative along the motions of (52) under the specified control and, thus, as a Lyapunov function,

Result A.1: Relaxing the difference in torque (53) assures that τ_d, and therefore the internal cost δ, decays to zero from any nominally standing posture (Assumption D.1).

The exponential decay of the homogeneous (internal) torque solution leaves the second term of the cost function, $\epsilon = \tau_m^2 = (\tau_{m,p}+\tau_{m,h})^2$, determined by the gravitational torque field through $\tau_{m,p}$ (48), which can be minimized by bringing θ_m to a critical point of ζ_o. For $\phi \in \mathcal{U}$, the closest

[8] Without this dependence, the two controllers could be run sequentially.

FIGURE 6. X-RHex performing a reactive stand on rocks.

TABLE 3. Reactive stand power from seated position. Each row is an average of five trials, and idle ("hotel") power has been removed. First group started from a sitting posture, second group started from walking posture.

Terrain	Slope	Normal Power	Reactive Power	Change
Asphalt	None	6.02 W	3.64 W	39.6%
Rocks	Various	6.32 W	3.73 W	40.1%
Grass	−14.0° pitch, 11.1° roll	5.89 W	4.12 W	30.0%
Grass	1.2° pitch, 5.5° roll	11.43 W	4.34 W	62.0%
Dirt	18.8–19.9° pitch	22.50 W	4.01 W	82.2%
Carpet	None	36.63 W	3.97 W	89.2%
Smooth	10.6° pitch	15.55 W	3.98 W	74.4%
Rocks	Various	31.25 W	7.30 W	76.6%

critical point is a local maximum. Therefore, we consider minimizing the function $-\zeta_o$, and implement the quasi-static dynamics $\tilde{\theta}_m := \kappa_m \tau_m$, since this implies,[9]

$$-\dot{\zeta}_o = -D\zeta_o \cdot \dot{\theta}_m = \begin{cases} -m_b g \kappa_m \kappa_p |D\zeta_o|^2 & |\tilde{\theta}_m| \leq \kappa_\sigma \\ -\kappa_p \kappa_\sigma |D\zeta_o| & |\tilde{\theta}_m| > \kappa_\sigma \end{cases} \quad (54)$$

i.e., $-\zeta_0$ (a smooth positive definite function in the neighborhood of a maximum), has a negative definite derivative under the control input as it enters the dynamics (50), and therefore,

Result A.2: Fighting the mean torque (54) assures that θ_m converges to the local minimum of $-\zeta_0$, the local maximum of ζ_o, and therefore the external cost ϵ, decays to zero from any nominally standing posture (Assumption D.1).

Furthermore, as discussed in Section II-F, since quasi-statically rolling is the same as an equivalent stick leg, and the above proof holds for any leg angle and length so long as $\gamma_i > 0$, we find that,

Result A.3: The convergence of (53)–(54) holds even under rolling contact, and so either leg shape converges to near-zero cost.

Thus for this first behavior, either leg shape is acceptable.

4) EXPERIMENTAL RESULTS

We implement this controller on the robot by straightforward generalization of the difference torque controller (53), for each leg individually, and the mean torque controller (54), now applied to the mean of all six legs [13, Section III.D]. The controller was tested on a variety of terrains by having the robot execute a reactive stand from either a sitting or walking posture. Fig. 6 shows a test on a pile of rocks, and Table 3 summarizes the results.

Note that regardless of the initial conditions, the reactive power was reduced to around 4 W. In fact every trial except for one on the rocks reduced the power to below 5 W. In that outlier, with a final power usage of 21.2 W, the robot slipped partway through execution of the smart stand, and, as the current behavior executes for a fixed time, the robot did not have time to completely recover. Anecdotally, the entire robot can typically be turned off after this behavior runs and the robot remains standing (implying that the remaining 4 W may came from the control electronics or noise). Furthermore since the experiments that started from a walk contained a mixture of leg contact conditions (some legs on the rounded half and some on the toe), these results supports the claim that both round and stick legs converge to near-zero power under this controller.

[9]The coupling of $\tau_{m,h}$ adds a sign indefinite term to the top line, $-\alpha\kappa_m\kappa_p \frac{\gamma_2-\gamma_1}{2} D\zeta_o$, but α is exponentially driven to zero by (53).

B. PITCHING SENSOR SWEEP

The behavior developed in this section allows the robot to actuate around the pitch component of its body frame. While prior work has posed the problem and initiated an analysis [14] and empirical application [15] of such behaviors, both efforts introduced point solutions that focused on a single contact mode with ad-hoc geometry. Here the formal derivation of an expression for the pitch as an implicit function of the leg state, $\mathbf{h}_\phi(\theta)$, allows analytical solutions in any contact condition, with consequent formal insight into the implications of leg shape.

Section IV-B.1 uses the domains of the various quasi-static contact conditions for RHex (Section II-C, Fig. 4) and the implicit function for pitch based on the base kinematic constraint (Section II-D) as in (44) in order to evaluate across all contact conditions to find the maximum range (as shown in Fig. 7). This range is extended from about 10° of pitch when both legs are in rolling contact (as first discovered in [14]), to about 35° when all modes are considered, greatly increasing the view of the world afforded to any payload sensors. Furthermore Section IV-B.2 compares the torque (Section II-H) needed to hold a pitched pose with different leg shapes, finding that the rounded leg uses less power than the stick leg. Section IV-B.3 shows that the pitching rate is exactly controlled by the analytical expression (59), based on the closed-loop constraint (Section II-G), eliminating the need for a numerical solution to guarantee constant pitching velocity [14]. Finally, Section IV-B.4 checks the dynamic

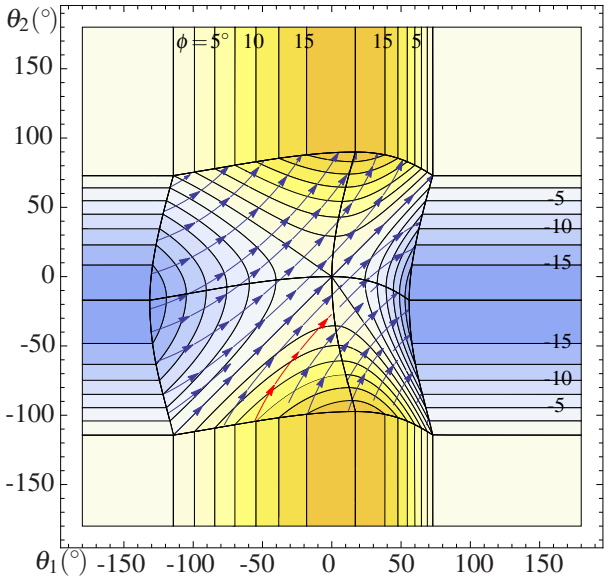

FIGURE 7. Contour plot of pitch ϕ as a function of θ_1 and θ_2, (55) over entire quasi-static configuration space (Fig. 4). Flow lines show constrained motion of the joints during double support (19). The red highlighted flow is solution from [14].

effects (Section II-J) to maintain the integrity of the sensory behavior by ensuring that the platform maintains frictional contact with the ground.

1) SCANNING RANGE

Within a given quasi-static contact mode (Fig. 4), pitch is an implicit function of the equality constraint (44), which for example in rolling contact on both legs (for simplicity written here for a symmetric robot, Assumption D.2),[10]

$$\mathbf{h}_\phi(\theta) = \arctan\left(\frac{4\ell + \rho(\sin(\theta_2) - \sin(\theta_1))}{\rho(\cos(\theta_2) - \cos(\theta_1))}\right). \qquad (55)$$

The value for ϕ for all quasi-static contact modes is shown in the contour plot of Fig. 7, as well as flow lines showing the constrained motion as a pushforward of a vector field over $\mathcal{Y}$ through (19).

The behavioral design problem is then to find the extrema of this pitch, formally set up as either a constrained optimization in each contact mode, or an unconstrained optimization over the combined implicit value for ϕ. This combined function is continuous as the active constraints in two neighboring contact conditions are subsets of the constraints on the boundary. The easiest way to solve this analytically is to choose $y = \theta_1 - \phi$, the global leg angle, and then parameterize the implicit function (55) in terms of y, (here shown for the case of a stick leg in front and body contact in the rear),[11]

$$\mathbf{h}_\phi(y) = \arcsin\frac{\rho_1\cos(y) - \rho_b}{\ell_1 + \ell_2} \qquad (56)$$

[10]Calculated by solving (44) for ϕ with the appropriate $\mathbf{a}$ (i.e. a concatenation of (42) for each leg).

[11]Calculated by solving (44) for ϕ with the appropriate $\mathbf{a}$ (i.e. a concatenation of (41) for the front and (43) in the rear) and replacing θ_1 with $y + \phi$.

FIGURE 8. Robot performing two pitching sensor sweeps with a planar laser scanner: (Left) upward ($\phi > 0$) to scan a staircase, (Right) downward ($\phi < 0$) to check for a cliff.

which is maximized at $\phi = \arcsin(\rho_1 - \rho_b/\ell_1 + \ell_2) \approx 17°$. It is clear from Fig. 7 that this maximal upward pitch of $\phi \approx 17°$ is achieved at $\theta_1 = 17°$ and $\theta_2 < -100°$, and from sitting ($\theta_1 = \theta_2 = -180°$) this pitch is only reachable when the rear body is sliding along the ground. Similarly the maximal downward pitch of $\phi \approx -17°$ is achieved at $\theta_2 = -17°$ and $\theta_1 < -130°$, i.e. when the front body is on the ground. This proves that,

Result B.1: The maximal pitching sensor sweep reaches $\phi = \pm\arcsin(\rho_1 - \rho_b/\ell_1 + \ell_2) \approx \pm 17°$ by using the sliding contact modes (56).

Such behaviors are shown in Fig. 8, where the robot is using a planar laser scanner to detect a stairwell and check for cliffs, as in [15]. However depending on the exact task a path through the double stance region may be useful in order to smoothly access both positive and negative pitches. If restricted to only rolling contact, then the maximal pitch is about 10°, as found in [14], and shown in Fig. 7.

2) TORQUE REQUIREMENT

While both round and stick legs reach these same extrema in pitch, the torque required is not the same. Under quasi-static operation the leg torque required to resist gravity is dictated by (16) and (23), however in these sliding contact modes $n = e = 1$, and so there are no internal forces, and $\mathbf{G}_s$ is directly invertible. Thus,

$$\tau_1 = -\mathbf{J}_h^T\mathbf{G}_s^{-1}\mathbf{F}_g$$

which can be compared for different leg shapes. Evaluating for round legs,[12]

$$\tau_1 = -\frac{\ell_2\rho_1 m_b g\cos(\phi)\sin(\theta_1 - \phi)}{2(\ell_1 + \ell_2)\cos(\phi) - \rho_1\sin(\theta_1 - \phi)} \qquad (57)$$

while for stick legs,[13]

$$\tau_1 = -\frac{\ell_2\rho_1 m_b g\cos(\phi)\sin(\theta_1 - \phi)}{(\ell_1 + \ell_2)\cos(\phi) - \rho_1\sin(\theta_1 - \phi)}. \qquad (58)$$

While both leg shapes have the same zero torque point (when the leg is vertical, as found for the previous behavior), in general,[14]

[12]Calculated with the appropriate $\mathbf{G}_s$ (i.e. a concatenation (84) of (82) for the front and (83) for the rear) and $\mathbf{J}_h$ (i.e. simply (86) for the front).

[13]Calculated with the appropriate $\mathbf{G}_s$ (i.e. a concatenation (84) of (81) for the front and (83) for the rear) and $\mathbf{J}_h$ (i.e. simply (85) for the front).

[14]Recall that these different contact conditions have different implicit relationships between ϕ and θ_1, however the factor of 2 in the denominator of (57) is the dominant factor.

Result B.2: A round leg (57) requires less torque to hold a pitched position than a stick leg (58) at the same angle.
This is easy to see intuitively, as the rounded leg has a shorter effective lever arm.

3) VELOCITY CONTROL

As the robot is pitching its sensor, the data can be correlated by recording the pitch as measured or calculated at each instant. However it may be necessary to sweep the sensor with some constant pitching speed. In [14] this was achieved by numerically inverting the forward kinematics to choose a leg angle velocity that produced the desired pitch velocity.

Here we take advantage of the analytical expression of $\mathbf{H}_o$ (19), the velocity Jacobian that arises from the closed-loop constraint. Take for example rolling contact for the front leg and body contact in the rear, and let $y := \theta_1$, then a desired pitch velocity of $\dot{\phi}_d$ can be achieved by setting the leg velocity,[15]

$$\dot{\phi} = \mathbf{H}_\phi \dot{\theta}_1 := \pi_\phi \mathbf{H} \dot{\theta}_1 \quad \Longleftrightarrow \quad \dot{\theta}_1 = (\mathbf{H}_\phi)^{-1} \dot{\phi},$$
$$\text{where} \quad (\mathbf{H}_\phi)^{-1} = \frac{\rho_1 \sin(\theta_1 - \phi) - 2(\ell_1 + \ell_2)\cos(\phi)}{\rho_1 \sin(\theta_1 - \phi)} \quad (59)$$

which can be implemented as an online feedback controller based on local measurements of θ_1 and ϕ, or can be calculated in advance numerically by using (18), (19), and thus,

Result B.3: A desired sensor pitch rate, $\dot{\phi}_d$ can be exactly achieved by joint velocity tracking control around the reference signal (59) as derived from the velocity Jacobian (19).

Note that the denominator of (19) goes to zero when $\theta_1 - \phi = 0$, i.e. when the leg is vertical, as in fact the maximal pitch has been reached and the velocity control can no longer be applied.

4) DYNAMICS

The maximum speed at which the scanning behavior can be executed is limited by the takeoff condition, $\mathbf{U}\lambda \geq 0$, (7), based on the dynamics, (39) i.e. above a certain speed ($\dot{y} := \dot{\theta}_1$) one of the contact points may lift off the ground. The maximum joint speed that avoids liftoff of either leg (with no torque, i.e. when the behavior reverses) is,

$$\begin{aligned} &\max \quad \dot{y} \\ &\text{s.t.} \quad \mathbf{U}\lambda \geq 0 \\ &\lambda = -\tilde{\mathbf{D}}_\lambda \dot{y} + \tilde{\mathbf{E}}_\lambda \\ &\tau = 0. \end{aligned}$$

This speed is shown in Fig. 9 for a subset of the configuration space, along with a trace of the solution from [14]. Now we can bound the speed of the system to be below the minimum over this range, which is about 300 °/s for the entire rolling contact range, or a little higher for most specific trajectories. In the rear body sliding contact case there is no solution to $\lambda_{2,n} = 0$, i.e. the front leg acting alone cannot lift the body off of the ground. However at high speeds the front leg loses contact, but those speeds are about twice that of the rolling contact case, and so, the maximum speed still consistent with full frictional contact is found numerically to be higher in the sliding modes (Fig. 9).

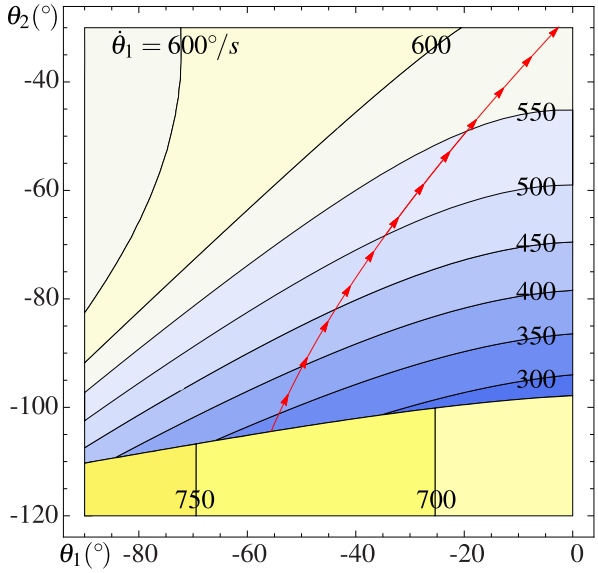

FIGURE 9. Leg speed ($\dot{\mathbf{y}} := \dot{\theta}_1$, in °/s) at takeoff. The discontinuity at around $\theta_2 = -110°$ occurs when the rear leg engages the ground. The red highlighted flow is solution from [14], but any behavior that engages only the front leg ($\theta_2 < -110$) may be run faster.

C. PITCH CONTROL IN LEAPING

Leaping with a low pitching velocity but high forward velocity (e.g. for gap crossing [17] or a pronking gait [18]) is very challenging for RHex because it entails in the high energy regime the delicate interaction of dynamics (Section II-I) with contact conditions (Section II-C) that we have already found to play a critical role in the quasi-static setting. For example, the pronk gait is known to have "severe pitch instability" on RHex [36], and as such several methods of pronking pitch control have been suggested[16]—modifying torques during stance, adjusting the leg angles before touchdown, and rear leg stubbing (rapid leg deceleration at the end of stance). The first strategy applies a differential torque between the motors [18], but under rigid assumptions the robot motion is constrained to a single DOF (as noted in the standing behavior). Even assuming leg compliance, this control authority is near-singular for typical leg angles for pronking [36].

The second strategy considers the plane generated by the toes when landing, as the robot quickly pitches until all toes are on the ground [18]. This effect can be canceled by setting the toes to be parallel to the ground [36], or exploited by adjusting it to a desired pitch [18]. This had limited success, as it, "appeared to disturb the robot's touchdown angles enough

[15]Calculated from (20) with $\mathbf{y}$ as given and the appropriate $\mathbf{A}$ (i.e. (17) with $\mathbf{G}_s$ and $\mathbf{J}_h$ as in (57).

[16]Of the first two, [37] notes, "Unfortunately ... neither method could be used successfully to control pitch during pronking."

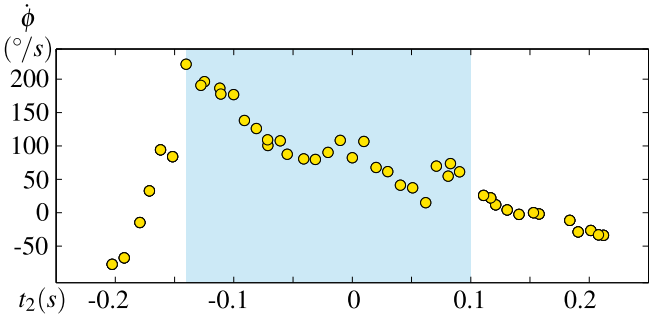

FIGURE 10. Pitching velocity ($\dot{\phi}$, in $^\circ/s$) at apex after a forward leap versus relative timing (t_2 in s). Highlighted region are leaps that included a double stance period.

to cause skidding" [37]. However the partial success of such strategies suggests that it may be beneficial in other ways, as it results in a splayed posture. The intuitive motivation to enforce symmetry between the legs does, at first, appear to control the pitch of the robot in stance as the parameterized free motion (19) has zero pitch. However when the friction constraints are considered (7), Section IV-C.1 proves that the front leg lifts off the ground first due to an unavoidable imbalance in toe normal forces (60), resulting in a positive pitch velocity. The same is not true when a fixed splay between the legs is applied, and Section IV-C.2 proves that a leap that uses such a splay inherently lowers the difference between front and rear normal forces, resulting in a lower pitch velocity (Fig. 10). The dynamics of the resulting rear leg support mode are higher dimensional and underactuated, but by following Section II-J we show in Section IV-C.3 that the faster the rear leg is moving, the more the robot pitches upwards (63). This effect explains the "stubbing" strategy used by some pronk controllers [36], [37], and is shown in an extreme case in Table 4 (based on [17]), where over 20° of pitch correction is generated by a last minute reversal in leg torque. Furthermore the liftoff conditions in this mode bound the possible forward velocity, which can be used to answer both leg and behavioral design questions (Section IV-C.4). This bound is lower for stick legs than rounded legs, and lower for level jumps than for pitched jumps, further supporting the need for a splayed leap.

Finally Section IV-C.5 tests the inertial effects of the nearly-massless legs, as derived from the robot dynamics. Leaping experiments verify that the legs can generate about 14° of body rotation (Fig. 14).

1) SYMMETRIC LIFTOFF CONDITIONS

Before the undesirable pitching velocity can be corrected, it is necessary to determine the source of the instability. Consider a symmetric robot (Assumption D.2) engaged in a "perfect" symmetric leap, i.e. with two stick legs locked in parallel ($\theta_1 \equiv \theta_2 \Rightarrow \phi \equiv 0$). This would at first glance appear to be a desirable target for stable pronking (as was used, e.g, in [36]), since there is no pitch and the pitch velocity is zeroed out by the infinitesimal kinematics,[17]

$$\mathbf{H}_\phi := \frac{\partial \phi}{\partial \theta_m} = \frac{2\rho^2 \sin(\theta_2 - \theta_1)}{\gamma_1 + \gamma_2} = 0$$

implying the same condition holds for the pitch acceleration, $\ddot{\phi}$. Why then does this gait fail? The answer lies in the liftoff conditions, $U\lambda \geq 0$,[18]

$$\lambda = -\mathbf{D}_\lambda \dot{\mathbf{q}} + \mathbf{E}_\lambda$$
$$= \begin{bmatrix} -\frac{\tau \tan(\theta_2)}{\ell} + \frac{\tau \cos(\theta_2)}{\rho} - \frac{1}{4} m_b g \sin(2\theta_2) - \frac{1}{2} m_b \rho \sin(\theta_2)\dot{\theta}_2^2 \\ \frac{\tau}{\ell} + \frac{m_b g}{4} + \frac{\tau \sin(\theta_2)}{\rho} + \frac{1}{4} m_b g \cos(2\theta_2) + \frac{1}{2} m_b \rho \cos(\theta_2)\dot{\theta}_2^2 \\ \frac{\tau \tan(\theta_2)}{\ell} + \frac{\tau \cos(\theta_2)}{\rho} - \frac{1}{4} m_b g \sin(2\theta_2) - \frac{1}{2} m_b \rho \sin(\theta_2)\dot{\theta}_2^2 \\ -\frac{\tau}{\ell} + \frac{m_b g}{4} + \frac{\tau \sin(\theta_2)}{\rho} + \frac{1}{4} m_b g \cos(2\theta_2) + \frac{1}{2} m_b \rho \cos(\theta_2)\dot{\theta}_2^2 \end{bmatrix}.$$

Thus the difference between the rear toe normal force (4th row, denoted "2n") and front toe normal force (2nd row, denoted "1n") is (note that in the normal force direction, $\mathbf{U} = -1$, as in (76)),

$$(\mathbf{U}\lambda)_{2n} - (\mathbf{U}\lambda)_{1n} = \frac{2\tau}{\ell} \tag{60}$$

i.e. the rear normal force is always larger than the front normal force, and so,

Result C.1: In a symmetric jump ($\theta_1 = \theta_2$), the front leg lifts off the ground first (60) as an unavoidable consequence of the dynamics (19) and contact constraint (7) (under Assumption D.2).

If this were a bilateral constraint (e.g. pin joint), the front leg would continue to pull down on the robot to maintain the neutral pitch that the closed-loop constraint suggests.

2) SPLAYED LIFTOFF CONDITIONS

For the non-symmetric jumping case ($\theta_1 \neq \theta_2$), the analytical solution to λ is complicated enough to obviate any benefit of direct visual inspection. However we can look at how the imbalance of (60) changes with the splay angle, $\theta_d := \mathbf{t}_d^T \theta$ (45) (under Assumptions D.2 and D.3),

$$\left.\frac{\partial \left((\mathbf{U}\lambda)_{2n} - (\mathbf{U}\lambda)_{1n}\right)}{\partial \theta_d}\right|_{\theta_d = 0} = -\frac{2\rho\tau \sin^2(\theta_m)}{\ell^2 \cos(\theta_m)} < 0 \tag{61}$$

(and numerically true even for I_b in Table 2), thus with otherwise equivalent conditions,

Result C.2: A positive splay angle (θ_d) reduces the imbalance between the front and rear normal forces (61) for RHex performing a forward leap (under Assumptions D.2 and D.3).

This splayed posture result is supported by the leaping dataset [49]. In those experiments, the robot performed a family of forward leaps while applying maximally available motor shaft torque with variations only in the relative timing of torque onset, t_2, which can be seen in that dataset to be well correlated with θ_d. Looking at the pitching moment at apex, as

[17] Calculated from (20) with $\mathbf{y} \equiv \theta_m$ (as in (47)) and the appropriate $\mathbf{A}$ (i.e. (17) where $\mathbf{G}_s$ is a concatenation (84) of (82) for each leg and $\mathbf{J}_h$ is block diagonal (87) with (86) for each leg), under Assumption D.2.

[18] Calculated from (33), using (88)–(92) and the same $\mathbf{A}$, or equivalently (39), under Assumption D.2.

listed in [49, Table I] and plotted in Fig. 10, it is clear that the pitching moment generated from a single leap decreases with increasing splay. Therefore a leap or pronk with a higher pitch ($\theta_d > 0$, i.e. below the main diagonal in the double rolling contact region of Fig. 7) on average incurs less deviation from that initial pitch during this first phase of the leap.

3) SINGLE LEG DYNAMICS

Once the front leg has lifted off the ground, the hybrid dynamics admit two degrees of freedom, and so we drop θ_1 from the state as under Assumption C.6, the massless front leg can have arbitrary position in the air, which would otherwise violate Assumption A.4. Note that this contact mode is not accessible quasi-statically, and as such is not shown in Fig. 4. Choosing $\mathbf{y} = [\theta_2, \phi]^T$, the constrained motion of (19) evaluated with $\mathbf{A}$ for a stick leg in the rear and no contact in the front,[19]

$$\dot{\mathbf{q}} = \mathbf{H}\dot{\mathbf{y}} = \begin{bmatrix} \dot{\theta}_2 \\ \rho_2 \cos(\theta_2 - \phi)(\dot{\theta}_2 - \dot{\phi}) - \ell_2 \sin(\phi)\dot{\phi} \\ \rho_2 \sin(\theta_2 - \phi)(\dot{\theta}_2 - \dot{\phi}) - \ell_2 \cos(\phi)\dot{\phi} \\ \dot{\phi} \end{bmatrix} \quad (62)$$

leading to the reduced dynamics of (35) for pitch,[20]

$$\begin{aligned} \ddot{\phi} &= -\tilde{\mathbf{D}}_\phi \dot{\mathbf{q}} + \tilde{\mathbf{E}}_\phi \\ &= \frac{\ell_2 m_b \cos(\theta_2)\left(\rho_2(\dot{\theta}_2 - \dot{\phi})^2 + \ell_2 \sin(\theta_2)\dot{\phi}^2\right)}{I_b + \ell_2^2 m_b \cos^2(\theta_2)} \\ &\quad + \frac{\tau_2(1 + \frac{\ell_2}{\rho_2}\sin(\theta_2)) - \ell_2 m_b g \cos(\theta_2)\cos(\theta_2 - \phi)}{I_b + \ell_2^2 m_b \cos^2(\theta_2)} \end{aligned} \quad (63)$$

where it is clear that,

Result C.3: Once the front leg has lifted off the ground, the harder the rear motor is pushing (τ_2), and the faster the rear leg is moving ($\dot{\theta}_2$, when $|\dot{\phi}| < |\dot{\theta}_2|$), the more the robot accelerates counterclockwise in pitch (i.e. "upwards", in the positive ϕ direction) (63).

Thus the controller design problem for a pronk-like leap becomes a balancing act between the conflicting criteria to both move quickly and maintain pitch control. Some pronk implementations on RHex reconcile this conflict by significantly reducing the torque at the end of stance, rapidly decelerating the leg [36], [37], essentially stubbing the toe in order to quickly correct the pitch. This toe stubbing effect was also anecdotally demonstrated as a leaping task in [17, Section IV-A.2]—here we present additional data from that experiment. To show the possibilities of this strategy in an extreme case, the apex state for two leaps, one with a strong toe stub and one without, are included in Table 4. This confirms that rapidly slowing down the rear leg at the end of a jump can induce a large pitch correction, greatly affecting the pitch velocity, though at the cost of 17% of the forward velocity.

[19] Calculated from (20) with $\mathbf{Y} = [1, 0, 0, 1]$ as given and the appropriate $\mathbf{A}$ (i.e. (17) where $\mathbf{G}_s$ is simply (81) and $\mathbf{J}_h$ is simply (85).

[20] Calculated from (35)–(37) with (88)–(92) and $\mathbf{H}$ as shown in (62).

TABLE 4. Comparison of forward leaps: the toe stub (Result C.3) has significant control authority over body pitch, in this extreme example changing the pitch by 24°.

Toe Stub?	ϕ	$\dot{\phi}$	$\lvert\dot{x}\rvert$	T
Without	10.4°	57°/s	1704 mm/s	11.4 J
With	−13.5°	−145°/s	1414 mm/s	8.3 J

4) IMPLICATIONS OF THE TAKEOFF CONDITION

As in the prior subsection, consider the case where the front leg has taken off and only the rear leg remains in contact. The friction cone (7) sets up an implicit bound on torque based on the contact forces (39),[21]

$$\begin{aligned} (\mathbf{U}\lambda)_{2n} \geq 0 \Rightarrow \\ \tau \geq \frac{\left\{ \begin{array}{l} I_b m_b \rho_2 \cos(\theta_2 - \phi)(\rho_2(\dot{\theta}_2 - \dot{\phi})^2 \\ +\ell_2 \sin(\theta_2)\dot{\phi} - g\cos(\theta_2 - \phi)) \end{array} \right\}}{\left\{ \begin{array}{l} \ell_2 m_b \cos\theta_2(\rho_2 \cos(\theta_2 - \phi) \\ +\ell_2 \sin\phi) - I_b \sin(\theta_2 - \phi) \end{array} \right\}} \end{aligned} \quad (64)$$

(here shown for a stick leg). Thus the faster the robot is moving ($\dot{\theta}_2$), the more torque is required to maintain contact, and so with any limited-torque actuator, the system speed exhibits a corresponding upper bound. However in general the faster an actuator is moving, the less torque it can produce. Applying a motor model of $\tau \leq \kappa_P \kappa_G (1 - \kappa_G \dot{\theta})$ [50] (where κ_P is proportional to peak motor power and κ_G is proportional to gear ratio), we can substitute for τ in (64) to get an equality that imposes a necessary condition for liftoff on the robot's state. This equality constraint can now be solved with a variety of different implicit functions to gain insight into the manner in which different design choices—either entailing physical parameters, or various behaviors entailing controllers which aim for different state space trajectories—can potentially influence the resulting conditions at liftoff. The simplest of these obtains by considering the equality to be a quadratic form in $\dot{\theta}$, so that the resulting root functions can be passed through the infinitesimal kinematics (62) yielding a closed-form expression for the maximum forward velocity at liftoff, here shown for mid-stance ($\theta_2 = 0$ and $\phi = 0$) with stick legs,

$$\begin{aligned} \dot{x} &= \frac{-\kappa_b + \sqrt{\kappa_b^2 + 4 I_b \kappa_c}}{2 I_b} \\ \kappa_b &:= \ell_2 \kappa_G^2 \kappa_P, \quad \kappa_c := \kappa_b \rho_2 \left(\frac{1}{\kappa_G} - \dot{\phi} \right) + \rho_2 g I_b. \end{aligned} \quad (65)$$

For rounded legs, the same maximum forward velocity is,

$$\dot{x} = \frac{-\kappa_b + \sqrt{\kappa_b^2 + 4\frac{I_b}{2}\kappa_c}}{2\frac{I_b}{2}}. \quad (66)$$

Fig. 11 shows this forward velocity bound for a robot with a stick leg and for a rounded leg across a range of leg and body angles typically found for stance. We conclude that,

[21] Calculated from (39)–(40) with (88)–(92) and $\mathbf{H}$ as shown in (62). Note that the denominator of (64) is positive under Assumption D.1, i.e. normal standing/running ranges, for values listed in Table 2.

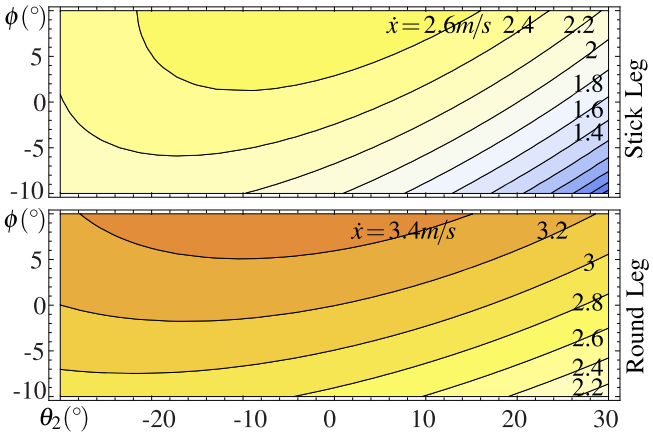

FIGURE 11. Forward velocity ($|\dot{x}|$, in m/s) at takeoff point of second (rear) leg for various leg angle θ_2 and pitch ϕ, assuming $\dot{\phi}=0$, and gear ratio $G=23$. On top, takeoff based on a stick leg, while on bottom takeoff based on a round leg.

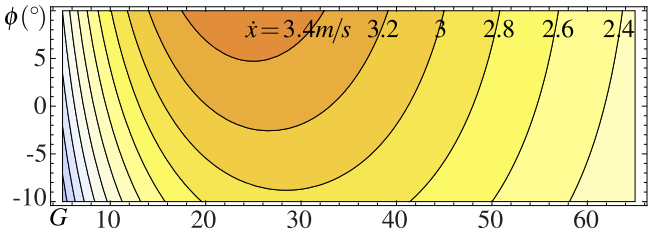

FIGURE 12. Forward velocity ($\dot{x}$, in m/s) at takeoff point of second (rear) leg under rolling contact for various gear ratios G and pitch ϕ, shown for $\dot{\phi}=0$, and optimal θ_2. Gear ratio for XRL is typically 23:1, just below the optimal of between 25–30.

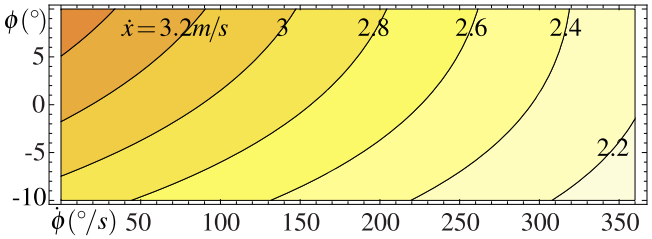

FIGURE 13. Forward velocity ($|\dot{x}|$, in m/s) at takeoff point of second (rear) leg under rolling contact for various pitching velocities $\dot{\phi}$ (in $^\circ/s$) and pitches ϕ (in $^\circ$), for optimal θ_2, and gear ratio $G=23$.

Result C.4: The dynamical bound on the forward speed is higher for rounded legs (66) than for stick legs (65).

as is true analytically for mid-stance[22] and therefore by smoothness for some neighborhood around that point, and is numerically shown to be at least 0.6 m/s faster over the entire range of Fig. 11 (all assuming $\dot{\phi}\approx 0$).

This bound is very rough as it does not consider compliance or damping (or in this figure, pitching velocity), but does shed considerable light on the new considerations that emerge in the dynamical regime whereby the rounded legs of RHex when running forward afford a higher speed limit, even at the point of mid-stance whereas, in contrast, quasi-statically the two morphological variants are equivalent (as described in Section II-F).

In contrast, the liftoff constraint (64) can be used in a more conventional numerical manner, for example determining the

$$\begin{aligned} \max \quad & \dot{x} \\ \text{s.t.} \quad & (\mathbf{U}\lambda)_{2n} \geq 0 \\ & \lambda = -\tilde{\mathbf{D}}_\lambda \dot{y} + \tilde{\mathbf{E}}_\lambda \\ & \tau \leq \kappa_P \kappa_G (1-\kappa_G \dot{\theta}) \end{aligned}$$

allowing $\dot{y}$ to vary. Specifically, note that for each ϕ in Fig. 11, there is a unique θ_2 that maximizes $\dot{x}$. As shown in Fig. 12 (shown for $\dot{\phi}\approx 0$), the optimal gear ratio lies somewhere around 25:1 depending on the pitch at take off, only slightly above the actual value of 23:1 for this robot.

Similarly, using this maximal takeoff point to eliminate θ_2 from (64) we can now test the desirability of $\dot{\phi}\approx 0$. Calculated numerically and shown in Fig. 13, we see that a positive pitch ϕ but small pitching velocity $\dot{\phi}$ (as results from a splayed posture) results in the highest maximum forward speed (numerically calculated based on Table 2).

[22]Compare (65)–(66) with the quadratic formula and note that the factor of 2 in the inertia ($\dot{x}^2$ term when written out in quadratic form) makes (65) smaller than (66) for any set of positive parameter values and $\dot{\phi} < 1/\kappa_G$, i.e. the motor no-load speed.

These maximal speed points are specific positions and velocities $(\mathbf{y}, \dot{\mathbf{y}})$ that may or may not be reachable—in fact as shown in Fig. 10 all of the jumps with double support in this way still had a non-zero positive pitching moment [49].

5) INERTIAL LEG EFFECTS

In the air, the dynamics of the robot are not restricted by the closed-loop constraint (12), as there are no contact forces, however conservation of angular momentum in the absence of external forces now imposes a nonholonomic constraint. Solving the dynamics as in Section II-I takes these conservation laws into account, ensuring that the time derivative of momentum is equal to the applied force, which here is zero. Recall that up until this point under Assumption C.6 we have used massless legs (as $m_l/m_b < 1\%$), but here we drop that assumption to test what effect the very light legs do have. The leg effectiveness [40] is defined as the body velocity per differential leg velocity, which can be calculated by placing the world reference frame, W, at the system center of mass and solving the conservation of angular momentum equation as follows (for a single leg),[23]

$$\begin{aligned} & \pi_\phi\left(\frac{\partial L}{\partial \dot{q}}\right) = \pi_\phi\left(\mathbf{Ad}_{g_{pw}}^T \widehat{\mathbf{M}}\begin{bmatrix}\dot{\theta}\\ \mathbf{V}_{op}^b\end{bmatrix}\right) = 0 \Rightarrow \\ & \varepsilon_n := \frac{\dot{\phi}}{\dot{\theta}_1} = -\frac{I_l + m_r\left((\frac{\rho_1}{2})^2 - \ell_1\frac{\rho_1}{2}\sin\theta_1\right)}{I_b + I_t + m_r\left(\ell_1^2 + (\frac{\rho_1}{2})^2 - 2\ell_1(\frac{\rho_1}{2})\sin\theta_1\right)} \\ & m_r := \frac{m_b m_l}{m_b + m_l} \end{aligned} \tag{67}$$

[23]Calculated with $\pi\mathbf{g}_{pw} := \frac{m_l}{m_l+m_b}\pi\mathbf{g}_{pl_1}$. Note that the conservation of momentum laws apply only to body velocities at the center of mass, as used here.

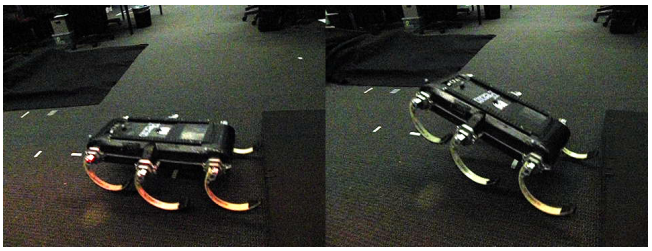

FIGURE 14. Robot state just prior to touchdown after two jumps: (Left) the legs completely recirculated clockwise, (Right) the legs went directly to the final angle counterclockwise.

which is the same as [40], up to notation. Note that the effectiveness is shape dependent—the relationship between leg velocity and body velocity is not constant over all θ. However an interesting simplification arises when two legs equally spaced from the robot COM (Assumption D.2) are controlled so as to be locked in parallel, $\theta_1(t) \equiv \theta_2(t)$,

$$\varepsilon_n := \frac{\dot{\phi}}{\dot{\theta}_1} = -\frac{2I_l + m_{r2}(\frac{\rho_1}{2})^2}{I_b + 2I_l + 2m_l\ell_1 + m_{r2}\frac{\rho_1}{2}}$$
$$m_{r2} := \frac{m_b(2m_l)}{m_b + (2m_l)} \tag{68}$$

i.e. the configuration dependence goes away. With all six legs included, the effectiveness for RHex is only $\varepsilon_n = 0.035$, though it is almost twice a naïve estimate of $\frac{6I_l}{I_b} = 0.018$ (see Table 2).

To verify the inertial effects of the legs, the robot performed a single jump (as in [17]) and the legs were sent to a given position, but in one case they were controlled to recirculate completely, while in the other they were not. Thus between the two tests the leg angles θ differ by exactly 360°. This resulted in a difference in body pitch of 14° (median taken across 5 jumps of each type), as shown in Fig. 14. Thus the measured effectiveness is $\varepsilon_m = 14/360 = 0.039$, quite close to what the model predicts, and critically,

Result C.5: The legs act as inertial tails and, when locked in phase, can produce a body rotation of ϵ_n (68) for each complete rotation they execute during flight (Fig. 14).

V. CONCLUSION

We have presented a formal framework for the generation of quasi-static and dynamic equations of motion for legged robots across multiple contact conditions. This framework matches as closely as possible the modeling decisions typically used for the analysis of multi-fingered hands, thereby highlighting the similarities and differences between the two classes of problems. The resulting systematic, unified and general methodology for modeling all contact conditions of a jointed, partly actuated, rigid-bodied mechanism that can move by generating ground reaction forces against a lumped parameter substrate promotes analysis of a rich variety of behaviors for common place scenarios that arise as legged robots leave the laboratory and enter the real world.

After the tutorial leading up to a "master equation" (33), we illustrate the utility of this methodology for behavior design in the context of a specifically imagined episode in an autonomous mission of a RHex robot. Along the way to this equation we recall from the manipulation literature the notion of a grasp map, $\mathbf{G}$ (13) whose null space introduces a transparent account of internal and external forces, yielding a simple, general, and provably correct algorithm (53)–(54) for standing still over unknown terrain with minimal power draw (Table 3). Reducing the influence of the highly varied mechanics across the multiplicity of contact conditions to the appearance of one term (17) promotes a straightforward comparison of the quality of exteroception (55)–(59) across all quasi-statically reachable configurations, enabling the robot to act as as an active laser wall/cliff detector (Fig. 8). Formal reasoning about the intrinsic conflict between leg torques and liftoff speed (60)–(66) sheds new light on the problem of how to leap forward most energetically without pitching. Finally, in each of these task settings, the formal nature of the results affords clear answers to morphological design questions such as the consequences of leg shape. Tracing back more systematically similar threads between the various design parameter values (Table 2) and the behavioral results they promote or constrain ought to be useful in future redesign of this and other legged robots.

Looking ahead, it is useful to compare the results of this paper with those resulting from a more combinatorially focused study of how to use ground reaction forces in legged self-manipulation. In [17] we examined the dynamic effects different strings of multiple contact modes could impose assuming very simple controls. In contrast, this paper has focused on the effects of much more finely varied control policies implemented within individual (and, sometimes, pairwise sequences of) contact modes. Legged self-manipulation will require a combination of both styles of planning and control: the combinatorial challenge of planning sequences of modes, and the refinement of control strategy within each mode, will both be critical in general for extracting the most capability legged robots can achieve in a complex world.

APPENDIX

A. KINEMATIC CONSTRAINTS

The base constraint (8) may be expanded as,

$$\mathbf{x}_{c_k} = \pi_{c_k}(\mathbf{g}_{c_k w}(\mathbf{q})) = \pi_{c_k}\left(\mathbf{g}_{c_k s_k}(\mathbf{q}) \cdot \mathbf{g}_{s_k w}(\mathbf{x})\right)$$

where,

$$\mathbf{g}_{c_k s_k}(\mathbf{q}) := \mathbf{g}_{c_k f_k}(\mathbf{q}) \cdot \mathbf{g}_{f_k s_k}(\theta)$$
$$\mathbf{g}_{s_k w}(\mathbf{x}) := \mathbf{g}_{s_k p} \cdot \mathbf{g}_{pw}(\mathbf{x})$$

however note that while $\mathbf{g}_{c_k f_k}$ depends on $\mathbf{q}$, the projection $\pi_{c_k}(\mathbf{g}_{c_k f_k})$ does not vary over time (i.e. it may be thought of as being parameterized by the initial value, $\mathbf{q}_a(0)$, but not a time varying function of $\mathbf{q}$). This frictional restriction is much clearer when expressed as a velocity constraint, $\mathbf{B}_{c_k}^T \mathbf{V}_{c_k f_k}^s \equiv 0$,

which is one reason most multi-fingered manipulation texts often skip the base constraint and directly apply a velocity or force constraint (including refs. [1]–[6]).

The velocity constraint equation (11) is proven in twist coordinates by using the following identities (see [1, p. 59] for proof of (69) and Section F, below, for a proof of (70)),

$$\mathbf{V}^s_{ac} = \mathbf{V}^s_{ab} + \mathbf{Ad}_{g_{ab}}\mathbf{V}^s_{bc} \tag{69}$$
$$\mathbf{V}^s_{ab} = -\mathbf{V}^b_{ba} \tag{70}$$

[1, Prop. 2.14, Lemma 2.16], and the friction constraint,

$$\mathbf{B}^T_{c_k}\mathbf{V}^s_{c_kf_k} \equiv 0 \tag{71}$$

[1, Eqn. 5.9] (ensuring no motion in the constrained directions) and so,

$$\begin{aligned}
0 &= \frac{d}{dt}\mathbf{a}_k \circ \mathbf{q}_a = \mathbf{B}^T_{c_k}\dot{\mathbf{g}}_{c_kw}\cdot\mathbf{g}^{-1}_{c_kw}\cdot\mathbf{g}_{c_kw} \Rightarrow 0 = \mathbf{B}^T_{c_k}\mathbf{V}^s_{c_kw} \\
&= \mathbf{B}^T_{c_k}(\mathbf{V}^s_{c_ks_k} + \mathbf{Ad}_{g_{c_ks_k}}\mathbf{V}^s_{s_kw}) \\
\mathbf{V}^s_{c_ks_k} &= \mathbf{V}^s_{c_kf_k} + \mathbf{Ad}_{g_{c_kf_k}}\mathbf{V}^s_{f_ks_k} = -\mathbf{V}^b_{f_kc_k} - \mathbf{Ad}_{g_{c_kf_k}}\mathbf{V}^b_{s_kf_k} \\
\mathbf{V}^s_{s_kw} &= \mathbf{V}^s_{s_kp} + \mathbf{Ad}_{g_{s_kp}}\mathbf{V}^s_{pw} = 0 - \mathbf{Ad}_{g_{s_kp}}\mathbf{V}^b_{wp} \\
0 &= \mathbf{B}^T_{c_k}(-\mathbf{Ad}_{g_{c_kf_k}}\mathbf{V}^b_{s_kf_k} - \mathbf{Ad}_{g_{c_ks_k}}\mathbf{Ad}_{g_{s_kp}}\mathbf{V}^b_{wp}) \\
&= -\mathbf{B}^T_{c_k}\mathbf{Ad}_{g_{c_kf_k}}(\mathbf{q})\mathbf{J}^b_{s_kf_k}(\theta)\dot{\theta} - \mathbf{B}^T_{c_k}\mathbf{Ad}_{g_{c_kp}}(\mathbf{q})\mathbf{R}^T_{wp}\dot{\mathbf{x}}.
\end{aligned}$$

An alternate proof of (11) is given here using a homogeneous representations of velocity, $\hat{\mathbf{V}} := (\mathbf{V})^\wedge$, by using the following identities (in addition to (70), proven below),

$$\hat{\mathbf{V}}^s_{ab} := \dot{\mathbf{g}}_{ab}\mathbf{g}^{-1}_{ab}$$
$$\left(\mathbf{Ad}_{g_{ab}}\mathbf{V}^s_{bc}\right)^\wedge = \mathbf{g}_{ab}\hat{\mathbf{V}}^s_{bc}\mathbf{g}^{-1}_{ab}$$

[1, Eqn. 2.53, Lemma 2.13] (and indeed all of [1, Section 2.4]), and the friction constraint (71) so,

$$\begin{aligned}
0 &= \frac{d}{dt}\mathbf{a}_k \circ \mathbf{q}_a \\
&= \mathbf{B}^T_{c_k}\left(\dot{\mathbf{g}}_{c_kf_k}\mathbf{g}_{f_ks_k}\mathbf{g}_{s_kw} + \mathbf{g}_{c_kf_k}\dot{\mathbf{g}}_{f_ks_k}\mathbf{g}_{s_kw}\right. \\
&\qquad \left.+\mathbf{g}_{c_kf_k}\mathbf{g}_{f_ks_k}\mathbf{g}_{s_kp}\dot{\mathbf{g}}_{pw}\right)^\vee \\
&= \mathbf{B}^T_{c_k}\left((\dot{\mathbf{g}}_{c_kf_k}\mathbf{g}^{-1}_{c_kf_k} + \mathbf{g}_{c_kf_k}\dot{\mathbf{g}}_{f_ks_k}\mathbf{g}^{-1}_{f_ks_k}\mathbf{g}^{-1}_{c_kf_k}\right. \\
&\qquad \left.+\mathbf{g}_{c_kp}\dot{\mathbf{g}}_{pw}\mathbf{g}^{-1}_{pw}\mathbf{g}^{-1}_{c_kp})\mathbf{g}_{c_kw}\right)^\vee \\
\Rightarrow 0 &= \mathbf{B}^T_{c_k}(\mathbf{V}^s_{c_kf_k} + \mathbf{Ad}_{g_{c_kf_k}}\mathbf{V}^s_{f_ks_k} + \mathbf{Ad}_{g_{c_kp}}\mathbf{V}^s_{pw}) \\
&= 0 - \mathbf{B}^T_{c_k}\mathbf{Ad}_{g_{c_kf_k}}\mathbf{J}^b_{s_kf_k}\dot{\theta} - \mathbf{B}^T_{c_k}\mathbf{Ad}_{g_{c_kp}}\mathbf{R}^T_{wp}\dot{\mathbf{x}} = \mathbf{A}_k(\mathbf{q})\dot{\mathbf{q}}.
\end{aligned}$$

B. GRASP MAP AND HAND JACOBIAN

The definition of the grasp map (13) is often given in terms of body velocity, $\mathbf{V}^b_{po}$, but computation of the dynamics is easiest in some local coordinates, $\dot{\mathbf{x}}$. Here we have also defined a grasp map in terms of the more relevant body velocity $\mathbf{V}^b_{op}$. These various versions of the grasp map are, of course, equivalent as summarized here:

$$\mathbf{G}^T_s\mathbf{R}^T_{wp}\dot{\mathbf{x}} = \mathbf{G}^T_s\mathbf{V}^b_{wp} = \mathbf{G}^T_s\mathbf{V}^b_{op} = \mathbf{G}^T\mathbf{V}^b_{po}.$$

For further notes on this see [1, Eqn. 6.18] as opposed to [1, Eqn. 5.15], discussion on [1, pp. 279, 283], and paragraph surrounding [6, Eqn. 28.1].

As for the hand Jacobian, note that the contact wrenches (or twists) at one toe have no direct effect on joints on a different leg (hence the block diagonal structure of $\mathbf{J}_h$). The indirect effects are captured by the closed-loop constraint (11,12). That the legs can be decoupled in this way is less obvious than in the multi-finger manipulation case, where each finger is rigidly attached to a fixed inertial frame. This decoupling comes from Newton's third law of motion, that every action has an equal and opposite reaction, and thus we may calculate the joint torques equally well by adding up the effects on either side of the joint.

C. ROLLING CONTACT

As noted in Sec. II-F, the fact that RHex's legs are not simple sticks does not change any of the analysis thus far, it simply makes the $\mathbf{G}_s$ and $\mathbf{J}_h$ matrices more complicated. The free motion of the hip at any given moment under rolling contact is identical to the motion of an equivalent stick leg connecting the hip to the contact point.

To prove this, consider a point on the circumference of a circle as it rolls—it follows a cycloid path. If we first assume that the world frame W is attached to the ground at the toe when the robot is standing ($\theta = 0$), with the z axis pointing into the ground, then the hip location is $(x_c, z_c) := \pi\mathbf{g}_{ws}(0) = (0, -2\rho_h)$ (where $\rho_h := \rho_1/2$ is the leg radius) then the position of the hip as a function of the motor angle θ is,

$$x_c = \rho_h\theta + \rho_h\sin(\theta), \qquad z_c = -\rho_h - \rho_h\cos(\theta).$$

Note that the definition of θ used in this paper has the leg in contact on the rounded half of the leg when $\theta < 0$, i.e. the leg is on the rounded half before mid-stance, and on the toe afterwards (as opposed to other robots whose half-circle legs are used in the opposite direction [42]).

Now consider a virtual leg extending from the hip to the contact point. Let the angle that this virtual leg makes with vertical be ϑ and the leg length be ρ_l. The hip position relative to the true world frame at that moment, $(x_f, z_f) := \pi\mathbf{g}_{ws}(\vartheta)$, for a fixed leg of length ρ_l and angle ϑ is,

$$x_f = \rho_l\sin(\vartheta), \qquad z_f = -\rho_l\cos(\vartheta).$$

First note that the triangle consisting of the center of the leg, the hip, and the contact point must be isosceles, as two of the sides are length ρ_h, and the third length ρ_l. The angle at the center of the circle must then be $\pi - \theta$ as the supplementary angle is θ. Therefore by noting that the equal angles in that triangle are ϑ, we find that $\vartheta = \theta/2$.

Now the infinitesimal direction of free motion for each case (i.e. the tangent of the trajectory),

$$\begin{aligned}
\frac{\partial x_c}{\partial\theta} &= \rho_h + \rho_h\cos(\theta), & \frac{\partial z_c}{\partial\theta} &= \rho_h\sin(\theta) \\
\frac{\partial x_f}{\partial\vartheta} &= \rho_l\cos(\vartheta), & \frac{\partial z_f}{\partial\vartheta} &= \rho_l\sin(\vartheta) \\
\frac{\partial z_c}{\partial x_c} &= \frac{\sin(\theta)}{1+\cos(\theta)}, & \frac{\partial z_f}{\partial x_f} &= \frac{\sin(\vartheta)}{\cos(\vartheta)}
\end{aligned}$$

can be compared using the double angle identity to find,

$$\frac{\partial z_c}{\partial x_c} = \frac{2\sin(\vartheta)\cos(\vartheta)}{1+2\cos^2(\vartheta)-1} = \frac{\sin(\vartheta)}{\cos(\vartheta)} = \frac{\partial z_f}{\partial x_f}.$$

Therefore the twist direction is the same whether you follow the full cycloid curve, or at each instant follow a virtual leg. This property is much more general than just for half circle legs, as shown in [1, Chapter 5.6].

D. DYNAMICS

The generalized mass matrix, $\overline{\mathbf{M}}$, is derived by summing the contribution of each link,

$$\begin{aligned}
T &= \frac{1}{2}m_b||v^b_{wp}||^2 + \frac{1}{2}I_b||\omega^b_{wp}||^2 \\
&\quad + \sum_{i=1}^{\mathrm{n}}\left(\frac{1}{2}m_{l_i}||v^b_{wl_i}||^2 + \frac{1}{2}I_{l_i}||\omega^b_{wl_i}||^2\right) \\
&= \frac{1}{2}(\mathbf{V}^b_{wp})^T\mathbf{M}_b\mathbf{V}^b_{wp} + \sum_{i=1}^{\mathrm{n}}\frac{1}{2}(\mathbf{V}^b_{wl_i})^T\mathbf{M}_{l_i}\mathbf{V}^b_{wl}, \\
\mathbf{V}^b_{wl_i} &= \mathbf{Ad}_{g^{-1}_{pl_i}}\mathbf{V}^b_{wp} + \mathbf{V}^b_{pl_i} \\
T &= \frac{1}{2}(\mathbf{V}^b_{wp})^T\mathbf{M}_b\mathbf{V}^b_{wp} + \sum_{i=1}^{\mathrm{n}}\frac{1}{2}(\mathbf{Ad}_{g^{-1}_{pl_i}}\mathbf{V}^b_{wp} + \mathbf{V}^b_{pl_i})^T\mathbf{M}_{l_i} \\
&\quad \times(\mathbf{Ad}_{g^{-1}_{pl_i}}\mathbf{V}^b_{wp} + \mathbf{V}^b_{pl_i}) \\
&= \frac{1}{2}(\mathbf{V}^b_{wp})^T\mathbf{M}_b\mathbf{V}^b_{wp} + \sum_{i=1}^{\mathrm{n}}\left(\frac{1}{2}(\mathbf{V}^b_{pl_i})^T\mathbf{M}_{l_i}\mathbf{V}^b_{pl_i}\right. \\
&\qquad + (\mathbf{V}^b_{pl_i})^T\mathbf{M}_{l_i}\mathbf{Ad}_{g^{-1}_{pl_i}}\mathbf{V}^b_{wp} \\
&\qquad \left. + \frac{1}{2}(\mathbf{V}^b_{wp})^T\mathbf{Ad}^T_{g^{-1}_{pl_i}}\mathbf{M}_{l_i}\mathbf{Ad}_{g^{-1}_{pl_i}}\mathbf{V}^b_{wp}\right)
\end{aligned}$$

where both $\mathbf{Ad}_{g^{-1}_{pl_i}}$ and $\mathbf{J}_{l_i}$ both depend only on θ. Substituting $\mathbf{V}^b_{wp} = \mathbf{R}^T_{wp}\dot{\mathbf{x}}$ results in the inertia tensor given in (26).

The accelerations and constraint forces may be solved for as follows (33),

$$\begin{aligned}
&\overline{\mathbf{M}}(\theta,\phi)\ddot{\mathbf{q}} + \overline{\mathbf{C}}(\theta,\phi,\dot{\mathbf{q}})\dot{\mathbf{q}} + \overline{\mathbf{N}}(\theta,\phi) + \mathbf{A}^T(\theta,\phi)\lambda = \Upsilon(\tau) \\
&\begin{bmatrix}\overline{\mathbf{M}} & \mathbf{A}^T & \overline{\mathbf{C}} \\ \mathbf{A} & 0 & \dot{\mathbf{A}}\end{bmatrix}\begin{bmatrix}\ddot{\mathbf{q}} \\ \lambda \\ \dot{\mathbf{q}}\end{bmatrix} = \begin{bmatrix}\Upsilon - \overline{\mathbf{N}} \\ 0\end{bmatrix} \\
&\begin{bmatrix}\overline{\mathbf{M}} & \mathbf{A}^T \\ \mathbf{A} & 0\end{bmatrix}\begin{bmatrix}\ddot{\mathbf{q}} \\ \lambda\end{bmatrix} = \begin{bmatrix}\Upsilon - \overline{\mathbf{N}} \\ 0\end{bmatrix} - \begin{bmatrix}\overline{\mathbf{C}} \\ \dot{\mathbf{A}}\end{bmatrix}\dot{\mathbf{q}} \\
&\begin{bmatrix}\ddot{\mathbf{q}} \\ \lambda\end{bmatrix} = \begin{bmatrix}\overline{\mathbf{M}} & \mathbf{A}^T \\ \mathbf{A} & 0\end{bmatrix}^{-1}\begin{bmatrix}\Upsilon - \overline{\mathbf{N}} \\ 0\end{bmatrix} - \begin{bmatrix}\overline{\mathbf{M}} & \mathbf{A}^T \\ \mathbf{A} & 0\end{bmatrix}^{-1}\begin{bmatrix}\overline{\mathbf{C}} \\ \dot{\mathbf{A}}\end{bmatrix}\dot{\mathbf{q}}.
\end{aligned}$$

Some dimensional analysis—the dynamics provides q equations, and the constraint equation provides c. Total, there are $2q + c$ unknowns, so in non-singular configurations we can solve for the $q + c$ unknowns $\ddot{\mathbf{q}}$ and λ in terms of the q remaining variables, $\dot{\mathbf{q}}$, as shown above. Note that this does not require $\overline{\mathbf{M}}$ be invertible, which is not the case with massless legs, or require $\mathbf{J}_h$ be invertible (as with [1, Eqn. 6.22]), which never is the case with "simple" legs like on RHex. Instead this method solves for both the system accelerations and constraint forces at the same time by inverting a block matrix that includes $\overline{\mathbf{M}}$ and $\mathbf{A}$ that in general is non-singular so long as $\mathrm{rank}(\overline{\mathbf{M}}) + \mathrm{rank}(\mathbf{A}) \geq \mathrm{q} + \mathrm{c}$, or $\mathrm{rank}(\overline{\mathbf{M}}) \geq \mathrm{e} = \mathrm{q} - \mathrm{c}$ and the constraints are non-singular (this is equivalent to the requirement that the mass matrix of the reduced dynamics, $\tilde{\mathbf{M}}$, to be defined in the next section, be full rank).

Now putting the whole system together we arrive at the differential equation (and splitting up the rows of $\mathbf{D}$ and $\mathbf{E}$ as suggested by the subscript),

$$\begin{aligned}
\frac{d}{dt}\begin{bmatrix}\dot{\mathbf{q}} \\ \mathbf{q}\end{bmatrix} &= \begin{bmatrix}-\mathbf{D}_{\ddot{q}} & 0 \\ \mathbf{Id}_{\mathrm{q}} & 0\end{bmatrix}\begin{bmatrix}\dot{\mathbf{q}} \\ \mathbf{q}\end{bmatrix} + \begin{bmatrix}\mathbf{E}_{\ddot{q}} \\ 0\end{bmatrix} \\
\lambda &= -\mathbf{D}_\lambda\dot{\mathbf{q}} + \mathbf{E}_\lambda.
\end{aligned} \tag{72}$$

As used in [1, Eqn. 6.23], and [6, Eqn. 28.20], the dynamics may re-written in twist coordinates (though only after we have derived them in local coordinates), where (33) becomes,

$$\begin{aligned}
&\widehat{\mathbf{M}}(\theta)\dot{\nu} + \widehat{\mathbf{C}}(\theta,\nu)\nu + \widehat{\mathbf{N}}(\theta,\phi) + \begin{bmatrix}-\mathbf{J}_h \\ \mathbf{G}_s\end{bmatrix}\lambda = \Upsilon(\tau), \\
&\nu := \begin{bmatrix}\dot{\theta} \\ \mathbf{V}^b_{op}\end{bmatrix},
\end{aligned} \tag{73}$$

where $\widehat{\mathbf{M}}$ is the combined body inertia tensor as given in (25), while $\widehat{\mathbf{C}}$, and $\widehat{\mathbf{N}}$ have been suitably rotated by $\mathbf{R}_{wp}$. However the lower line of (72) must reflect $\dot{\mathbf{x}} = \mathbf{R}_{wp}\mathbf{V}^b_{op}$.

If $\overline{\mathbf{M}}$ is invertible, the Lagrange multipliers may be solved for first and then used to calculate $\ddot{\mathbf{q}}$,

$$\begin{aligned}
\lambda &= (\mathbf{A}\overline{\mathbf{M}}^{-1}\mathbf{A}^T)^{-1}\left(\mathbf{A}\overline{\mathbf{M}}^{-1}(\Upsilon - \overline{\mathbf{C}}\dot{\mathbf{q}} - \overline{\mathbf{N}}) + \dot{\mathbf{A}}\dot{\mathbf{q}}\right), \\
\ddot{\mathbf{q}} &= \overline{\mathbf{M}}^{-1}\left(\Upsilon - \overline{\mathbf{C}}\dot{\mathbf{q}} - \overline{\mathbf{N}} - \mathbf{A}^T\lambda\right),
\end{aligned}$$

[1, Eqn. 6.5, 6.6].

E. REDUCED DYNAMICS

The reduced dynamics can be found by using the Lagrangian written in the reduced coordinates,

$$\begin{aligned}
\tilde{T}(\mathbf{y},\dot{\mathbf{y}}) &:= \frac{1}{2}\dot{\mathbf{y}}^T\mathbf{H}^T(\mathbf{h}(\mathbf{y}))\overline{\mathbf{M}}(\mathbf{h}(\mathbf{y}))\mathbf{H}(\mathbf{h}(\mathbf{y}))\dot{\mathbf{y}} = \frac{1}{2}\dot{\mathbf{y}}^T\tilde{\mathbf{M}}\dot{\mathbf{y}} \\
\tilde{V}(\mathbf{y}) &:= V(\mathbf{h}(\mathbf{y})) \\
\tilde{L}(\mathbf{y},\dot{\mathbf{y}}) &= \frac{1}{2}\dot{\mathbf{y}}^T\tilde{\mathbf{M}}(\mathbf{h}(\mathbf{y}))\dot{\mathbf{y}} - \tilde{V}(\mathbf{h}(\mathbf{y}))
\end{aligned}$$

and following along as above, or by noting that $\mathbf{H}^T\mathbf{A}^T = 0$ and working from (32),

$$\begin{aligned}
\overline{\mathbf{M}}(\theta)\ddot{\mathbf{q}} + \overline{\mathbf{C}}(\theta,\dot{\theta})\dot{\mathbf{q}} + \overline{\mathbf{N}}(\theta,\phi) + \mathbf{A}^T(\theta,\phi)\lambda &= \Upsilon \\
\mathbf{H}^T\overline{\mathbf{M}}\ddot{\mathbf{q}} + \mathbf{H}^T\overline{\mathbf{C}}\dot{\mathbf{q}} + \mathbf{H}^T\overline{\mathbf{N}} + \mathbf{H}^T\mathbf{A}^T\lambda &= \mathbf{H}^T\Upsilon \\
\mathbf{H}^T\overline{\mathbf{M}}(\mathbf{H}\ddot{\mathbf{y}} + \dot{\mathbf{H}}\dot{\mathbf{y}}) + \mathbf{H}^T\overline{\mathbf{C}}\mathbf{H}\dot{\mathbf{y}} + \mathbf{H}^T\overline{\mathbf{N}} + 0 &= \mathbf{H}^T\Upsilon \\
\tilde{\mathbf{M}}\ddot{\mathbf{y}} + \tilde{\mathbf{C}}\dot{\mathbf{y}} + \tilde{\mathbf{N}} &= \tilde{\Upsilon}
\end{aligned}$$

leading to (35) and summarized as,

$$\frac{d}{dt}\begin{bmatrix}\dot{\mathbf{y}} \\ \mathbf{q}\end{bmatrix} = \begin{bmatrix}-\tilde{\mathbf{D}}(\mathbf{q},\dot{\mathbf{y}}) & 0 \\ \mathbf{H}(\mathbf{q}) & 0\end{bmatrix}\begin{bmatrix}\dot{\mathbf{y}} \\ \mathbf{q}\end{bmatrix} + \begin{bmatrix}\tilde{\mathbf{E}}(\mathbf{q}) \\ 0\end{bmatrix}. \tag{74}$$

To recover the Lagrange multipliers, using the pseudoinverse $\mathbf{A}^*\mathbf{A}^T = \mathbf{Id}_c$ as chosen in (40),

$$\begin{aligned}\lambda &= \mathbf{A}^*(\Upsilon - \overline{\mathbf{M}}\ddot{\mathbf{q}} - \overline{\mathbf{C}}\dot{\mathbf{q}} - \overline{\mathbf{N}}) \\ &= \mathbf{A}^*(\Upsilon - (\overline{\mathbf{M}}\mathbf{H})\ddot{\mathbf{y}} - (\overline{\mathbf{M}}\dot{\mathbf{H}} + \overline{\mathbf{C}}\mathbf{H})\dot{\mathbf{y}} - \overline{\mathbf{N}}) \\ &= \mathbf{A}^*(\mathbf{Id}_q - \overline{\mathbf{M}}\mathbf{H}(\mathbf{H}^T\overline{\mathbf{M}}\mathbf{H})^{-1}\mathbf{H}^T) \\ &\quad \times(\Upsilon - (\overline{\mathbf{M}}\dot{\mathbf{H}} + \overline{\mathbf{C}}\mathbf{H})\dot{\mathbf{y}} - \overline{\mathbf{N}}) \\ &= \mathbf{A}^*(\Upsilon - (\overline{\mathbf{M}}\dot{\mathbf{H}} + \overline{\mathbf{C}}\mathbf{H})\dot{\mathbf{y}} - \overline{\mathbf{N}}).\end{aligned}$$

Note that the other term in (40) has an interesting (though here unused) interpretation, as $(\overline{\mathbf{M}}\mathbf{H})^*\mathbf{A}^T = \mathbf{0}$ implies that when $\dot{\mathbf{q}}^T \in (\overline{\mathbf{M}}\mathbf{H})^*$, $\mathbf{A}\dot{\mathbf{q}} = \mathbf{0}$, i.e. its rows are the state velocities that imparts no contact force whatsoever. Furthermore since $(\overline{\mathbf{M}}\mathbf{H})^*(\overline{\mathbf{M}}\mathbf{H}) = \mathbf{Id}_e$, such velocities also impart unit compliment momentum in the reduced system, i.e. $\mathbf{H}^T\overline{\mathbf{M}}\dot{\mathbf{q}}$ is a unit basis vector.

F. PROOFS OF LEMMAS

The proof of [1, Lemma 2.16],

$$\begin{aligned}\mathbf{V}^b_{ab} &= -\mathbf{V}^s_{ba}, \\ \mathbf{V}^b_{ab} &= -\mathbf{Ad}_{g_{ba}}\mathbf{V}^b_{ba},\end{aligned}$$

uses the following properties of rigid transformations and skew symmetric matrices,

$$\begin{aligned}\mathbf{R}_{ab} &= \mathbf{R}_{ba}^{-1} = \mathbf{R}_{ba}^T, \\ \mathbf{R}^T(\mathbf{p})^\wedge\mathbf{R} &= (\mathbf{R}^T\mathbf{p})^\wedge, \qquad (\mathbf{p})^\wedge\mathbf{R} = \mathbf{R}(\mathbf{R}^T\mathbf{p})^\wedge, \\ \dot{\mathbf{R}}\mathbf{R}^T &= -(\dot{\mathbf{R}}\mathbf{R}^T)^T, \\ \mathbf{R}(\mathbf{S})^\vee &= (\mathbf{RSR}^T)^\vee, \\ (\mathbf{p})^\wedge\mathbf{q} &= -(\mathbf{q})^\wedge\mathbf{p}, \\ \mathbf{g}_{ab}^{-1} &= (-\mathbf{R}_{ab}^T\mathbf{p}_{ab}, \mathbf{R}_{ab}^T) = (\mathbf{p}_{ba}, \mathbf{R}_{ba}) = \mathbf{g}_{ba},\end{aligned}$$

[1, Sec. 2.2.1, 2.4] and the definitions

$$\begin{aligned}\mathbf{V}^s_{ab} &= \begin{bmatrix} -\dot{\mathbf{R}}_{ab}\mathbf{R}_{ab}^T\mathbf{p}_{ab} + \dot{\mathbf{p}}_{ab} \\ (\dot{\mathbf{R}}_{ab}\mathbf{R}_{ab}^T)^\vee \end{bmatrix}, \\ \mathbf{V}^b_{ab} &= \begin{bmatrix} \mathbf{R}_{ab}^T\dot{\mathbf{p}}_{ab} \\ (\mathbf{R}_{ab}^T\dot{\mathbf{R}}_{ab})^\vee \end{bmatrix}, \\ \mathbf{Ad}_{g_{ab}} &= \begin{bmatrix} \mathbf{R}_{ab} & (\mathbf{p}_{ab})^\wedge\mathbf{R}_{ab} \\ 0 & \mathbf{R}_{ab} \end{bmatrix}, \\ \mathbf{V}^s_{ab} &= \mathbf{Ad}_{g_{ab}}\mathbf{V}^b_{ab},\end{aligned}$$

[1, Eqn. 2.58–2.61] and so the second part of the Lemma is proven as,

$$\begin{aligned}-\mathbf{Ad}_{g_{ba}}\mathbf{V}^b_{ba} &= -\begin{bmatrix} \mathbf{R}_{ba} & (\mathbf{p}_{ba})^\wedge\mathbf{R}_{ba} \\ 0 & \mathbf{R}_{ba} \end{bmatrix}\begin{bmatrix} \mathbf{R}_{ba}^T\dot{\mathbf{p}}_{ba} \\ (\mathbf{R}_{ba}^T\dot{\mathbf{R}}_{ba})^\vee \end{bmatrix} \\ &= -\begin{bmatrix} \mathbf{R}_{ba}\mathbf{R}_{ba}^T\dot{\mathbf{p}}_{ba} + (\mathbf{p}_{ba})^\wedge\mathbf{R}_{ba}(\mathbf{R}_{ba}^T\dot{\mathbf{R}}_{ba})^\vee \\ \mathbf{R}_{ba}(\mathbf{R}_{ba}^T\dot{\mathbf{R}}_{ba})^\vee \end{bmatrix} \\ &= -\begin{bmatrix} \dot{\mathbf{p}}_{ba} + \mathbf{R}_{ba}(\mathbf{R}_{ba}^T\mathbf{p}_{ba})^\wedge(\mathbf{R}_{ba}^T\dot{\mathbf{R}}_{ba})^\vee \\ (\mathbf{R}_{ba}(\mathbf{R}_{ba}^T\dot{\mathbf{R}}_{ba})\mathbf{R}_{ba}^T)^\vee \end{bmatrix} \\ &= -\begin{bmatrix} \dot{\mathbf{p}}_{ba} - \dot{\mathbf{R}}_{ba}\mathbf{R}_{ba}^T\mathbf{p}_{ba} \\ (\dot{\mathbf{R}}_{ba}\mathbf{R}_{ba}^T)^\vee \end{bmatrix} \\ &= -\begin{bmatrix} (-\dot{\mathbf{R}}_{ab}^T\mathbf{p}_{ab} - \mathbf{R}_{ab}^T\dot{\mathbf{p}}_{ab}) - \dot{\mathbf{R}}_{ab}^T\mathbf{R}_{ab}(-\mathbf{R}_{ab}^T\mathbf{p}_{ab}) \\ (\dot{\mathbf{R}}_{ab}^T\mathbf{R}_{ab})^\vee \end{bmatrix} \\ &= \begin{bmatrix} \mathbf{R}_{ab}^T\dot{\mathbf{p}}_{ba} \\ (\mathbf{R}_{ab}^T\dot{\mathbf{R}}_{ab})^\vee \end{bmatrix} \\ &= \mathbf{V}^b_{ab}\end{aligned}$$

and thus the first part is also proven by combining this with the definition of $\mathbf{Ad}_{g_{ba}}$,

$$\mathbf{V}^s_{ba} = \mathbf{Ad}_{g_{ba}}\mathbf{V}^b_{ba} = -\mathbf{V}^b_{ab}.$$

G. VALUES FOR RHex

Based on the specification of Section III-A.

From Section II-C, the point contacts with friction at the toes implies a projection $\pi_{c_k} := \pi$ down to the linear components, x and z, which thus leads to a planar wrench basis of,

$$\mathbf{B}_{c_k} := \begin{bmatrix} 1 & 0 \\ 0 & 1 \\ 0 & 0 \end{bmatrix}, \quad k \in 1, 2 \tag{75}$$

corresponding to tangential and normal forces in the contact frame. The corresponding friction cone (7) is (where recall that $\mathcal{C}_k$ is defined with the $\mathbf{z}$ axis pointing into the ground),

$$\mathbf{U}_k\lambda_{c_k} := \begin{bmatrix} \pm 1 & \mu_k \\ 0 & -1 \end{bmatrix}\begin{bmatrix} \lambda_{kt} \\ \lambda_{kn} \end{bmatrix} \geq 0, \quad k \in 1, 2 \tag{76}$$

where the sign of the coefficient on the tangent components is selected to be the opposite of the sign of λ_t, or alternatively both signs may be included in separate rows, and μ_k is the usual static friction coefficient.

When the body contacts the ground, the sliding contact implies a projection $\pi_{c_k} := \pi_z$ down to only the normal component, z, and thus has a wrench basis of,

$$\mathbf{B}_{b_k} := \begin{bmatrix} 0 \\ 1 \\ 0 \end{bmatrix}, \quad k \in 3, 4 \tag{77}$$

and the friction cone is,

$$\mathbf{U}_k\lambda_{c_k} := \begin{bmatrix} -1 \end{bmatrix}\begin{bmatrix} \lambda_{kn} \end{bmatrix} \geq 0, \quad k \in 3, 4. \tag{78}$$

The combined $\mathbf{U}$ for all k contacts is then defined as (7),

$$\mathbf{U}\lambda := \begin{bmatrix} \mathbf{U}_1 & 0 & 0 \\ 0 & \ddots & 0 \\ 0 & 0 & \mathbf{U}_\mathrm{k} \end{bmatrix}\begin{bmatrix} \lambda_{c_1} \\ \vdots \\ \lambda_{c_\mathrm{k}} \end{bmatrix} \geq 0. \tag{79}$$

From Section II-D, the active components $\mathbf{a}_k$ of the base kinematic constraint are shown in (41)–(43), which combine to form $\mathbf{a}$ in each contact mode,

$$\mathbf{a} := \begin{bmatrix} \mathbf{a}_1 \\ \vdots \\ \mathbf{a}_\mathrm{k} \end{bmatrix}. \tag{80}$$

From Section II-E, the component of the self-manipulation grasp map for each toe contact ($0 \leq \theta_k - \phi < \pi, k \in 1, 2$) is

$$\overline{\mathbf{M}} = \begin{bmatrix} \frac{1}{4}m_l\rho_1^2+I_l & 0 & \frac{1}{2}\cos(\theta_1\text{-}\phi)m_l\rho_1 & \frac{1}{2}\sin(\theta_1\text{-}\phi)m_l\rho_1 & I_l+\frac{1}{4}m_l\rho_1(\rho_1-2\sin(\theta_1)\ell_1) \\ & \frac{1}{4}m_l\rho_2^2+I_l & \frac{1}{2}\cos(\theta_2-\phi)m_l\rho_2 & \frac{1}{2}\sin(\theta_2-\phi)m_l\rho_2 & I_l+\frac{1}{4}m_l\rho_2(2\sin(\theta_2)\ell_2+\rho_2) \\ & & m_b+2m_l & 0 & \frac{1}{2}m_l(2\sin(\phi)(\ell_2-\ell_1)+\cos(\theta_1-\phi)\rho_1+\cos(\theta_2-\phi)\rho_2) \\ & & & m_b+2m_l & \frac{1}{2}m_l(2\cos(\phi)(\ell_2-\ell_1)+\sin(\theta_1-\phi)\rho_1+\sin(\theta_2-\phi)\rho_2) \\ & & & & I_b-\sin(\theta_1)m_l\ell_1\rho_1+\sin(\theta_2)m_l\ell_2\rho_2+2I_l+m_l\left(\ell_1^2+\ell_2^2+\frac{\rho_1^2+\rho_2^2}{4}\right) \end{bmatrix}$$

$$\overline{\mathbf{C}} = \frac{m_l}{2}\begin{bmatrix} 0 & 0 & \sin(\theta_1\text{-}\phi)\,\dot{\phi}\rho_1 & -\cos(\theta_1\text{-}\phi)\,\dot{\phi}\rho_1 & -\big(\cos(\theta_1\text{-}\phi)\dot{z}-\sin(\theta_1\text{-}\phi)\dot{x}-\cos(\theta_1)\,\dot{\phi}\ell_1\big)\rho_1 \\ 0 & 0 & \sin(\theta_2\text{-}\phi)\,\dot{\phi}\rho_2 & -\cos(\theta_2\text{-}\phi)\,\dot{\phi}\rho_2 & -\big(\cos(\theta_2\text{-}\phi)\dot{z}-\sin(\theta_2\text{-}\phi)\dot{x}+\cos(\theta_2)\,\dot{\phi}\ell_2\big)\rho_2 \\ -\sin(\theta_1\text{-}\phi)\rho_1\dot{\theta}_1 & -\sin(\theta_2\text{-}\phi)\rho_2\dot{\theta}_2 & 0 & 0 & \dot{\phi}(2\cos(\phi)(\ell_2-\ell_1)+\sin(\theta_1\text{-}\phi)\rho_1+\sin(\theta_2\text{-}\phi)\rho_2) \\ \cos(\theta_1\text{-}\phi)\rho_1\dot{\theta}_1 & \cos(\theta_2\text{-}\phi)\rho_2\dot{\theta}_2 & 0 & 0 & -\dot{\phi}(2\sin(\phi)(\ell_2-\ell_1)+\cos(\theta_1\text{-}\phi)\rho_1+\cos(\theta_2\text{-}\phi)\rho_2) \\ \rho_1\begin{pmatrix}\cos(\theta_1\text{-}\phi)\dot{z}-\sin(\theta_1\text{-}\phi)\dot{x} \\ -\cos(\theta_1)\ell_1(\dot{\phi}+\dot{\theta}_1)\end{pmatrix} & \rho_2\begin{pmatrix}\cos(\theta_2\text{-}\phi)\dot{z}-\sin(\theta_2\text{-}\phi)\dot{x} \\ +\cos(\theta_2)\ell_2(\dot{\phi}+\dot{\theta}_2)\end{pmatrix} & \begin{pmatrix}-\sin(\theta_1\text{-}\phi)\rho_1\dot{\theta}_1 \\ -\sin(\theta_2\text{-}\phi)\rho_2\dot{\theta}_2\end{pmatrix} & \begin{pmatrix}\cos(\theta_1\text{-}\phi)\rho_1\dot{\theta}_1 \\ +\cos(\theta_2\text{-}\phi)\rho_2\dot{\theta}_2\end{pmatrix} & \cos(\theta_2)\ell_2\rho_2\dot{\theta}_2-\cos(\theta_1)\ell_1\rho_1\dot{\theta}_1 \end{bmatrix}$$

FIGURE 15. Mass and Coriolis tensors. Note that in the interest of compactness only the upper half of the symmetric $\overline{\mathbf{M}}$ is shown.

thus,

$$\mathbf{G}_{s,k} = \begin{bmatrix} -\cos\phi & \sin\phi \\ -\sin\phi & -\cos\phi \\ \ell_k\sin\phi-\rho_k\cos(\theta_k-\phi) & \ell_k\cos\phi-\rho_k\sin(\theta_k-\phi) \end{bmatrix} \tag{81}$$

while the component of the grasp map for rolling contact $(-\pi < \theta_k - \phi < 0, k \in 1, 2)$ is,

$$\mathbf{G}_{s,k} = \begin{bmatrix} -\cos\phi & \sin\phi \\ -\sin\phi & -\cos\phi \\ \ell_k\sin\phi-\frac{\rho_k}{2}(1+\cos(\theta_k-\phi)) & \ell_k\cos\phi-\frac{\rho_k}{2}\sin(\theta_k-\phi) \end{bmatrix}. \tag{82}$$

The component of the grasp map for each body contact $k \in 3, 4$ is thus,

$$\mathbf{G}_{s,k} = \begin{bmatrix} \sin\phi \\ -\cos\phi \\ \ell_k\cos\phi \end{bmatrix}. \tag{83}$$

A complete grasp map is then the concatenation of all active components (14),

$$\mathbf{G}_s := \begin{bmatrix} \mathbf{G}_{s,1} & \dots & \mathbf{G}_{s,\mathrm{k}} \end{bmatrix}. \tag{84}$$

The hand Jacobian for legs in toe contact $(0 < \theta_k - \phi < \pi, k \in 1, 2)$ is thus,

$$\mathbf{J}_{h,k} = \begin{bmatrix} -\rho_k\cos(\theta_k-\phi) \\ -\rho_k\sin(\theta_k-\phi) \end{bmatrix} \tag{85}$$

while the hand Jacobian for rolling contact $(-\pi < \theta_k - \phi < 0, k \in 1, 2)$,

$$\mathbf{J}_{h,k} = \begin{bmatrix} -\frac{\rho_k}{2}(1+\cos(\theta_k-\phi)) \\ -\frac{\rho_k}{2}\sin(\theta_k-\phi) \end{bmatrix} \tag{86}$$

and the hand Jacobian is zero for $k \in 3, 4$. A complete hand Jacobian is then a block diagonal of all active components,

$$\mathbf{J}_h := \begin{bmatrix} \mathbf{J}_{h,1} & 0 & 0 \\ 0 & \ddots & 0 \\ 0 & 0 & \mathbf{J}_{h,\mathrm{k}} \end{bmatrix}. \tag{87}$$

The combined velocity constraint matrix $\mathbf{A}$ for each contact mode is defined from these components (17). For example the combined constraint $\mathbf{A}$ in the mode shown in Fig. 3 (front leg rolling, rear leg toe contact, no body contact) is,

$$\mathbf{A} = \begin{bmatrix} -\mathbf{J}_h & \mathbf{G}_s^T\mathbf{R}_{pw}^T \end{bmatrix}$$

$$= \begin{bmatrix} \frac{\rho_1}{2}(1+\cos(\theta_1-\phi)) & 0 & -1 & 0 & \ell_1\sin\phi-\frac{\rho_1}{2}(1+\cos(\theta_1-\phi)) \\ \frac{\rho_1}{2}\sin(\theta_1-\phi) & 0 & 0 & -1 & \ell_1\cos\phi-\frac{\rho_1}{2}\sin(\theta_1-\phi) \\ 0 & \rho_2\cos(\theta_2-\phi) & -1 & 0 & -\ell_2\sin\phi-\rho_2\cos(\theta_2-\phi) \\ 0 & \rho_2\sin(\theta_2-\phi) & 0 & -1 & -\ell_2\cos\phi-\rho_2\sin(\theta_2-\phi) \end{bmatrix}.$$

From Section II-G and II-H, see examples worked out in Section IV.

From Section II-I, the combined mass matrix (26) and Coriolis matrix (30) are shown in Fig. 15, Eqn. (81), (82). Recall that these are the same in every contact state.

However when assuming massless legs, $\overline{\mathbf{M}}$ is much simpler,

$$\overline{\mathbf{M}}_{massless} = \begin{bmatrix} 0 & 0 & 0 & 0 & 0 \\ 0 & 0 & 0 & 0 & 0 \\ 0 & 0 & m_b & 0 & 0 \\ 0 & 0 & 0 & m_b & 0 \\ 0 & 0 & 0 & 0 & I_b \end{bmatrix} \tag{88}$$

and $\overline{\mathbf{C}}_{massless}$ is all zeros.

The potential energy is (recall that z points "down"),

$$V = -m_b g z \tag{89}$$

and thus the nonlinear forces (gravity) are,

$$\overline{\mathbf{N}} = \begin{bmatrix} 0 \\ 0 \\ 0 \\ -m_b g \\ 0 \end{bmatrix} \tag{90}$$

while the body wrench due to gravity is (recall that the body wrench is the negative of the object wrench),

$$\mathbf{F}_g = -\mathbf{R}_{wp}^T\overline{\mathbf{N}}_o = \begin{bmatrix} -m_b g\sin\phi \\ m_b g\cos\phi \\ 0 \end{bmatrix}. \tag{91}$$

The applied force is,

$$\Upsilon = \begin{bmatrix} \tau_1 \\ \tau_2 \\ 0 \\ 0 \\ 0 \end{bmatrix}. \tag{92}$$

From Section II-J, the constituent matrices are different in each contact mode and parameterization of the closed-loop parameter, but can be derived from (75)–(92).

ACKNOWLEDGMENTS

The authors would like to thank past and present members of Kod*lab, in particular G. C. Haynes, S. Burden, M. T. Hale, B. D. Ilhan, T. Herrmann, J. Sheng, and S. Revzen, as well as the authors of [1], [14], [18], [36], and finally the reviewers who provided insightful comments and questions.

REFERENCES

[1] R. M. Murray, Z. Li, and S. S. Sastry, *A Mathematical Introduction to Robotic Manipulation*. Boca Raton, FL: CRC Press, 1994.

[2] M. T. Mason and J. J. Kenneth Salisbury, *Robot Hands and the Mechanics of Manipulation*. Cambridge, MA: MIT Press, 1985.

[3] A. Bicchi and V. Kumar, "Robotic grasping and contact: A review," in *IEEE Int. Conf. Robotics and Automation*, vol. 1, 2000, pp. 348–353.

[4] A. M. Okamura, N. Smaby, and M. R. Cutkosky, "An overview of dexterous manipulation," in *IEEE Int. Conf. Robotics and Automation*, vol. 1, 2000, pp. 255–262.

[5] M. T. Mason, *Mechanics of Robotic Manipulation*. Cambridge, MA: MIT Press, Aug. 2001.

[6] B. Siciliano and O. Khatib, *Handbook of Robotics*. New York: Springer, 2008.

[7] Y. Fujimoto and A. Kawamura, "Simulation of an autonomous biped walking robot including environmental force interaction," *IEEE Robot. Automat. Mag.*, vol. 5, no. 2, pp. 33–42, 1998.

[8] U. Saranlı, M. Buehler, and D. E. Koditschek, "RHex: A Simple and Highly Mobile Hexapod Robot," *Int. J. Robotics Research*, vol. 20, no. 7, pp. 616–631, 2001.

[9] G. C. Haynes, J. Pusey, R. Knopf, A. M. Johnson, and D. E. Koditschek, "Laboratory on legs: an architecture for adjustable morphology with legged robots," in *Unmanned Systems Technology XIV*, vol. 8387, no. 1. SPIE, 2012, p. 83870W.

[10] I. W. Hunter, J. M. Hollerbach, and J. Ballantyne, "A comparative analysis of actuator technologies for robotics," *Robotics Review*, vol. 2, pp. 299–342, 1992.

[11] J. D. Madden, "Mobile robots: Motor challenges and materials solutions," *Science*, vol. 318, no. 5853, p. 1094 âĂŞ1097, Nov 2007.

[12] D. Dunn-Rankin, E. Leal, and D. Walther, "Personal power systems," *Progress in Energy and Combustion Science*, vol. 31, no. 5–6, p. 422âĂŞ465, 2005.

[13] A. M. Johnson, G. C. Haynes, and D. E. Koditschek, "Standing self-manipulation for a legged robot," in *IEEE/RSJ Int. Conf. Intelligent Robots and Systems*, Algarve, Portugal, Oct. 2012, pp. 272–279.

[14] E. Sayginer, T. Akbey, Y. Yazicioglu, and A. Saranlı, "Task oriented kinematic analysis for a legged robot with half-circular leg morphology," in *IEEE Int. Conf. Robotics and Automation*, May 2009, pp. 4088 –4093.

[15] A. M. Johnson, M. T. Hale, G. C. Haynes, and D. E. Koditschek, "Autonomous legged hill and stairwell ascent," in *IEEE Int. Workshop Safety, Security, and Rescue Robotics*, Nov. 2011, pp. 134–142.

[16] R. R. Burridge, A. A. Rizzi, and D. E. Koditschek, "Sequential composition of dynamically dexterous robot behaviors," *Int. J. Robotics Research*, vol. 18, no. 6, pp. 534–555, 1999.

[17] A. M. Johnson and D. E. Koditschek, "Toward a vocabulary of legged leaping," in *IEEE Int. Conf. Robotics and Automation*, May 2013, pp. 2553–2560.

[18] D. McMordie and M. Buehler, "Towards pronking with a hexapod robot," in *Int. Conf. Climbing and Walking Robots*, Karlsruhe, Germany, Sept. 2001, pp. 659–666.

[19] C. Chevallereau, J. W. Grizzle, and C.-L. Shih, "Asymptotically stable walking of a five-link underactuated 3-d bipedal robot," *IEEE Trans. Robot.*, vol. 25, no. 1, pp. 37–50, 2009.

[20] M. Yim, J. Reich, and A. A. Berlin, "Two approaches to distributed manipulation," in *Distributed Manipulation*, K. Böhringer and H. Choset, Eds. Springer, 2000, pp. 237–261.

[21] A. Shapiro, E. Rimon, and J. W. Burdick, "Passive force closure and its computation in compliant-rigid grasps," in *IEEE/RSJ Int. Conf. Intelligent Robots and Systems*, 2001, pp. 1769–1775.

[22] B. Beigzadeh, M. N. Ahmadabadi, A. Meghdari, and A. Akbarimajd, "A dynamic object manipulation approach to dynamic biped locomotion," *Robotics and Autonomous Systems*, vol. 56, no. 7, pp. 570 – 582, 2008.

[23] R. Featherstone, *Rigid body dynamics algorithms*. New York: Springer, 2008.

[24] J. Kerr and B. Roth, "Analysis of multifingered hands," *Int. J. Robotics Research*, vol. 4, no. 4, pp. 3–17, 1986.

[25] C. Cai and B. Roth, "On the spatial motion of a rigid body with point contact," in *IEEE Int. Conf. Robotics and Automation*, vol. 4, 1987, pp. 686–695.

[26] D. J. Montana, "The kinematics of contact and grasp," *Int. J. Robotics Research*, vol. 7, no. 3, pp. 17–32, 1988.

[27] N. Sankar, V. Kumar, and X. Yun, "Velocity and acceleration analysis of contact between three-dimensional rigid bodies," *J. Applied Mechanics*, vol. 63, no. 4, pp. 974–984, 1996.

[28] E. Rimon and J. W. Burdick, "Mobility of bodies in contact. I. A 2nd-order mobility index for multiple-finger grasps," *IEEE Trans. Robot. Autom.*, vol. 14, no. 5, pp. 696–708, 1998.

[29] K. Lynch, "Nonprehensile robotic manipulation: Controlability and planning," Ph.D. dissertation, Robotics Institute, Carnegie Mellon University, Pittsburgh, PA, March 1996.

[30] P. Holmes, R. J. Full, D. E. Koditschek, and J. Guckenheimer, "The dynamics of legged locomotion: Models, analyses, and challenges," *SIAM Review*, vol. 48, no. 2, pp. 207–304, 2006.

[31] R. Full and D. Koditschek, "Templates and anchors: Neuromechanical hypotheses of legged locomotion on land," vol. 202, no. 23, pp. 3325–3332, 1999.

[32] C. Li, T. Zhang, and D. I. Goldman, "Towards a terramechanics for legged locomotion on flowing ground," *Science*, vol. 339, pp. 1408–1412, 2013.

[33] E. Moore, D. Campbell, F. Grimminger, and M. Buehler, "Reliable stair climbing in the simple hexapod 'RHex'," in *IEEE Int. Conf. Robotics and Automation*, 2002.

[34] E. Z. Moore, "Leg design and stair climbing control for the RHex robotic hexapod," Ph.D. dissertation, McGill University, 2002.

[35] J. Burke, R. Murphy, M. Coovert, and D. Riddle, "Moonlight in miami: Field study of human-robot interaction in the context of an urban search and rescue disaster response training exercise," *Human–Computer Interaction*, vol. 19, no. 1-2, pp. 85–116, 2004.

[36] M. Ankaralı and U. Saranlı, "Control of underactuated planar pronking through an embedded spring-mass hopper template," *Autonomous Robots*, vol. 30, no. 2, pp. 217–231, 2011.

[37] D. McMordie, "Towards pronking with a hexapod robot," Master's thesis, McGill Univ., 2002.

[38] R. Balasubramanian, A. Rizzi, and M. T. Mason, "Legless locomotion: A novel locomotion technique for legged robots," *Int. J. Robotics Research*, vol. 27, no. 5, pp. 575 – 594, May 2008.

[39] T. Libby, T. Y. Moore, E. Chang-Siu, D. Li, D. J. Cohen, A. Jusufi, and R. J. Full, "Tail-assisted pitch control in lizards, robots and dinosaurs," *Nature*, vol. 481, no. 7380, pp. 181–184, 2012.

[40] A. M. Johnson, T. Libby, E. Chang-Siu, M. Tomizuka, R. J. Full, and D. E. Koditschek, "Tail assisted dynamic self righting," in *Int. Conf. Climbing and Walking Robots*, July 2012, pp. 611–620.

[41] A. M. Bloch, *Nonholonomic mechanics and control*. New York: Springer, 2003.

[42] A. Hoover, S. Burden, X.-Y. Fu, S. Sastry, and R. Fearing, "Bio-inspired design and dynamic maneuverability of a minimally actuated six-legged robot," in *IEEE Int. Conf. Biomedical Robotics and Biomechatronics*, Sept. 2010, pp. 869 –876.

[43] G. C. Haynes and D. E. Koditschek, "On the comparative analysis of locomotory systems with vertical travel," in *Int. Symp. Experimental Robotics*, Delhi, India, Dec. 2010.

[44] J. D. Weingarten, R. E. Groff, and D. E. Koditschek, "A framework for the coordination of legged robot gaits," in *IEEE Int. Conf. Robotics and Automation*, 2004, pp. 679–686.

[45] G. C. Haynes and A. A. Rizzi, "Gait regulation and feedback on a robotic climbing hexapod," in *Proc. Robotics: Science and Systems*, Philadelphia, USA, Aug. 2006.

[46] G. C. Haynes, "Gait regulation control techniques for robust legged locomotion," Ph.D. dissertation, Robotics Institute, Carnegie Mellon Univ., Pittsburgh, PA, May 2008.

[47] J. Sousa, V. Matos, and C. Peixoto dos Santos, "A bio-inspired postural control for a quadruped robot: An attractor-based dynamics," in *IEEE/RSJ Int. Conf. Intelligent Robots and Systems*, Oct. 2010, pp. 5329 –5334.

[48] L. Sentis, J. Park, and O. Khatib, "Compliant control of multicontact and center-of-mass behaviors in humanoid robots," *IEEE Trans. Robot.*, vol. 26, no. 3, pp. 483–501, 2010.

[49] A. M. Johnson and D. E. Koditschek, "Parametric jumping dataset on the RHex robot," Univ. of Pennsylvania, Tech. Rep., 2012.

[50] D. McMordie, C. Prahacs, and M. Buehler, "Towards a dynamic actuator model for a hexapod robot," in *IEEE Int. Conf. Robotics and Automation*, vol. 1, 2003.

AARON M. JOHNSON (S'06) received the B.S. degree from the Department of Electrical and Computer Engineering, Carnegie Mellon University, Pittsburgh, PA, USA, in 2008, and is currently pursuing the Ph.D. degree with the Department of Electrical and Systems Engineering, University of Pennsylvania, Philadelphia, PA, USA.

He is currently with the University of Pennsylvania, and was a Visiting Researcher with Boston Dynamics, Electrical Engineering Intern at iRobot, and a Research Engineer with Biorobotics Lab, Carnegie Mellon University. His current research interests include dynamic transitions, bio-inspired robotics, actuator modeling, and robot ethics.

Mr. Johnson was a Best Student Paper Finalist at the IEEE International Conference on Robotics and Automation, in 2013, as well as the Climbing and Walking Robots Conference, in 2012. He received the David Thuma Laboratory Project Award in 2008 from Carnegie Mellon University, and was an Honorable Mention for the Computing Research Association's Outstanding Undergraduate, in 2008.

DANIEL E. KODITSCHEK (S'80–M'83–SM'93–F'04) received the Ph.D. degree in electrical engineering from Yale University, New Haven, CT, USA, in 1983.

He served as a Faculty Member with the Department of Electrical Engineering, Yale University, for ten years, and then joined the Department of Electrical Engineering and Computer Science, University of Michigan, Ann Arbor, MI, USA, in 1993. He joined the University of Pennsylvania, Philadelphia, PA, USA, in January 2005, where he holds secondary appointments with the Departments of Computer and Information Science and Mechanical Engineering and Applied Mechanics. He is the Alfred Fitler Moore Professor and formerly a Chairman of electrical and systems engineering with the School of Engineering and Applied Science. His current research interests include robotics, the application of dynamical systems theory to intelligent machines, and nonlinear control.

Dr. Koditschek is a member of the AMS, ACM, MAA, SIAM, SICB, and Sigma Xi. He is a fellow of the AAAS. He received the Presidential Young Investigators Award in 1986.